

## Article

# Determinants for $\alpha 4\beta 2$ vs. $\alpha 3\beta 4$ Subtype Selectivity of Pyrrolidine-Based nAChRs Ligands: A Computational Perspective with Focus on Recent cryo-EM Receptor Structures

Francesco Bavo <sup>1,2</sup> , Marco Pallavicini <sup>1</sup>, Rebecca Appiani <sup>1</sup> and Cristiano Bolchi <sup>1,\*</sup>

<sup>1</sup> Dipartimento di Scienze Farmaceutiche, Università degli Studi di Milano, I-20133 Milano, Italy; francesco.bavo@sund.ku.dk (F.B.); marco.pallavicini@unimi.it (M.P.); rebecca.appiani@unimi.it (R.A.)

<sup>2</sup> Department of Drug Design and Pharmacology, University of Copenhagen, DK-2100 Copenhagen, Denmark

\* Correspondence: cristiano.bolchi@unimi.it

**Abstract:** The selectivity of  $\alpha 4\beta 2$  nAChR agonists over the  $\alpha 3\beta 4$  nicotinic receptor subtype, predominant in ganglia, primarily conditions their therapeutic range and it is still a complex and challenging issue for medicinal chemists and pharmacologists. Here, we investigate the determinants for such subtype selectivity in a series of more than forty  $\alpha 4\beta 2$  ligands we have previously reported, docking them into the structures of the two human subtypes, recently determined by cryo-electron microscopy. They are all pyrrolidine based analogues of the well-known  $\alpha 4\beta 2$  agonist *N*-methylprolinol pyridyl ether A-84543 and differ in the flexibility and pattern substitution of their aromatic portion. Indeed, the direct or water mediated interaction with hydrophilic residues of the relatively narrower  $\beta 2$  minus side through the elements decorating the aromatic ring and the stabilization of the latter by facing to the not conserved  $\beta 2$ -Phe119 result as key distinctive features for the  $\alpha 4\beta 2$  affinity. Consistently, these compounds show, despite the structural similarity, very different  $\alpha 4\beta 2$  vs.  $\alpha 3\beta 4$  selectivities, from modest to very high, which relate to rigidity/extendibility degree of the portion containing the aromatic ring and to substitutions at the latter. Furthermore, the structural rationalization of the rat vs. human differences of  $\alpha 4\beta 2$  vs.  $\alpha 3\beta 4$  selectivity ratios is here proposed.

**Keywords:** (*S*)-nicotine; nAChR; *N*-methyl-pyrrolidinyl; selectivity;  $\alpha 4\beta 2$ ;  $\alpha 3\beta 4$ ; docking; benzodioxane; cryo-EM



**Citation:** Bavo, F.; Pallavicini, M.; Appiani, R.; Bolchi, C. Determinants for  $\alpha 4\beta 2$  vs.  $\alpha 3\beta 4$  Subtype Selectivity of Pyrrolidine-Based nAChRs Ligands: A Computational Perspective with Focus on Recent cryo-EM Receptor Structures. *Molecules* **2021**, *26*, 3603. <https://doi.org/10.3390/molecules26123603>

Academic Editor: Clelia Dallanocce

Received: 3 May 2021

Accepted: 10 June 2021

Published: 12 June 2021

**Publisher's Note:** MDPI stays neutral with regard to jurisdictional claims in published maps and institutional affiliations.



**Copyright:** © 2021 by the authors. Licensee MDPI, Basel, Switzerland. This article is an open access article distributed under the terms and conditions of the Creative Commons Attribution (CC BY) license (<https://creativecommons.org/licenses/by/4.0/>).

## 1. Introduction

The development of ligands able to enhance the function of brain nicotinic acetylcholine receptors (nAChRs) has been, and still is, a pursued strategy to approach the treatment of cognitive deficits resulting from neurological and psychiatric disorders and some drug dependences [1]. The  $\alpha 4\beta 2$  nAChR, the major subtype in the brain, is primarily involved in such a strategy as its ligands, full or partial agonists, have shown a therapeutic potential as, for instance, antidepressants and drug cessation aids [2–4]. However, structural features relevant for full or partial agonism and for selectivity over the ganglionic  $\alpha 3\beta 4$  nicotinic subtype, which both condition the therapeutic range, remain two topical issues in SAR analysis and design of  $\alpha 4\beta 2$  ligands [5–7], undoubtedly more challenging than  $\alpha 4\beta 2$ - $\alpha 7$  selectivity, which is generally more inherent in both highly affinitive  $\alpha 4\beta 2$  and  $\alpha 7$  ligands [6,8]. On this matter, the structures of both human  $\alpha 4\beta 2$  and  $\alpha 3\beta 4$  receptors, recently determined by cryo-electron microscopy, can be a potent investigation tool suggesting new principles of agonist efficacy and, even more, of subtype selectivity [9,10].

The  $\alpha 3\beta 4$  subtype is mainly localized in the peripheral nervous system [11], where it mediates the effects on temperature, locomotor activity, and seizures elicitation and is also believed to be partially responsible for the cardiovascular and gastrointestinal liabilities of nicotine [12,13]. This subtype is highly concentrated also in a few brain regions and recent studies have suggested its role in influencing some behavioural effects of nicotine [14,15].

Structurally, nAChRs are transmembrane pentameric ligand-gated ion channels and are composed by five subunits assembled over a central aqueous pore, permeable to cations. Of particular note, until the recent resolution of the first full-length X-ray crystal structure the  $\alpha 4\beta 2$  nAChRs, three-dimensional information about the transmembrane domain, the pore structure and the binding site could only be obtained through homology modelling approaches [16–19]. Although models of the extracellular domain of nAChRs were considered reliable since based on X-ray crystal structures of the similar and homologous soluble acetylcholine binding protein (AChBP), the full length X-ray and cryo-EM structures of the human  $\alpha 4\beta 2$  and  $\alpha 3\beta 4$  nAChR substantially surpassed them.

In both subtypes, as observed in the cryo-EM structures and illustrated in Figure 1A, the orthosteric ligand ((*S*)-**nicotine**) binds in the extracellular domain (ECD) at each  $\alpha$ - $\beta$  interface (AB and DE interfaces). Each subunit contributes to enclosing the ligand with three loops: Loops A-C from the  $\alpha$  subunit (principal side) and loops D-F from the  $\beta$  subunit (complementary side). The pyrrolidine ring of (*S*)-**nicotine** is buried in the so-called “aromatic box”, a lipophilic cavity paved by loop A ( $\alpha 4$ -Tyr100 or  $\alpha 3$ -Tyr93) and D ( $\beta 2$ -Trp57 or  $\beta 4$ -Trp59) and surrounded by loop B ( $\alpha 4$ -Trp156 or  $\alpha 3$ -Trp149) and loop E ( $\beta 2$ -Leu121 or  $\beta 4$ -Leu123), which defines the back walls. The binding site is frontally closed by the flexible loop C ( $\alpha 4$ -Tyr197 and  $\alpha 4$ -Tyr204 or  $\alpha 3$ -Tyr190 and  $\alpha 3$ -Tyr197). Loop C packs on (*S*)-**nicotine** more tightly in the  $\alpha 3\beta 4$  subtype, rather than in the  $\alpha 4\beta 2$ , making the latter more compact. The top wall is lined by loop E ( $\beta 2$ -Val111 and  $\beta 2$ -Phe119 or  $\beta 4$ -Ile113 and  $\beta 4$ -Leu121). In addition to interacting through lipophilic contacts, the positively charged pyrrolidine establishes  $\pi$ -cation interactions with the aromatic box and a charge-assisted H-bond with the backbone carbonyl of  $\alpha 4$ -Trp156 or  $\alpha 3$ -Trp149. A structural water molecule has been experimentally demonstrated to bridge through H-bonds the pyridine nitrogen of (*S*)-**nicotine** with the backbone NH of Leu121, and was observed in the cryo-EM 6PV7 and in the previously reported X-ray crystal structure of an acetylcholine binding protein/nicotine complex [20,21].

In the last 15 years, we have designed and developed some series of chiral  $\alpha 4\beta 2$  ligands, full and partial agonists and antagonists [22], initially linking the N-methyl-2-pyrrolidinyl residue, typical of nicotinoids, to C(2) of 1,4-benzodioxane [23,24], a scaffold widely employed to design bioactive molecules [25–29] and, in this instance, to mimic the aryloxymethyl portion of prolinol aryl ethers, well known high-affinity  $\alpha 4\beta 2$  ligands such as **A-84543** [30] (Figure 1B; for benzodioxane scaffold numbering see (*S,R*)-**21** formula). Successive steps were the decoration of the benzodioxane by introducing substituents at its C(7) [31], deconstruction of the dioxane ring to give new phenyl and pyridyl ethers of prolinol [7,32], replacement of benzene with pyridine to give the four regioisomeric pyridodioxanes [5], and again benzodioxane decoration with substituents at C(6) and C(5) [33]. In each of these series of prolinol aryl ethers or benzodioxane/pyridodioxane derivatives some compounds, as exemplified in Figure 1, exhibited one to hundred nanomolar  $\alpha 4\beta 2$  affinity and some of these also from good to high functional and binding selectivity over the  $\alpha 3\beta 4$  subtype. Such diversified results for a large number of chiral compounds with relatively similar structures prompted us to study their interactions at the binding sites of the two human  $\alpha 4\beta 2$  and  $\alpha 3\beta 4$  receptors by docking them into the respective structures determined by cryo-electron microscopy (cryo-EM 6CNJ and 6PV7) [9,10].

Here, we report the results of this analysis, which can provide a rational support to the discussion of the  $\alpha 4\beta 2$ / $\alpha 3\beta 4$  selectivity structural requirements, a still open and debated issue in the nicotinic ligands research.

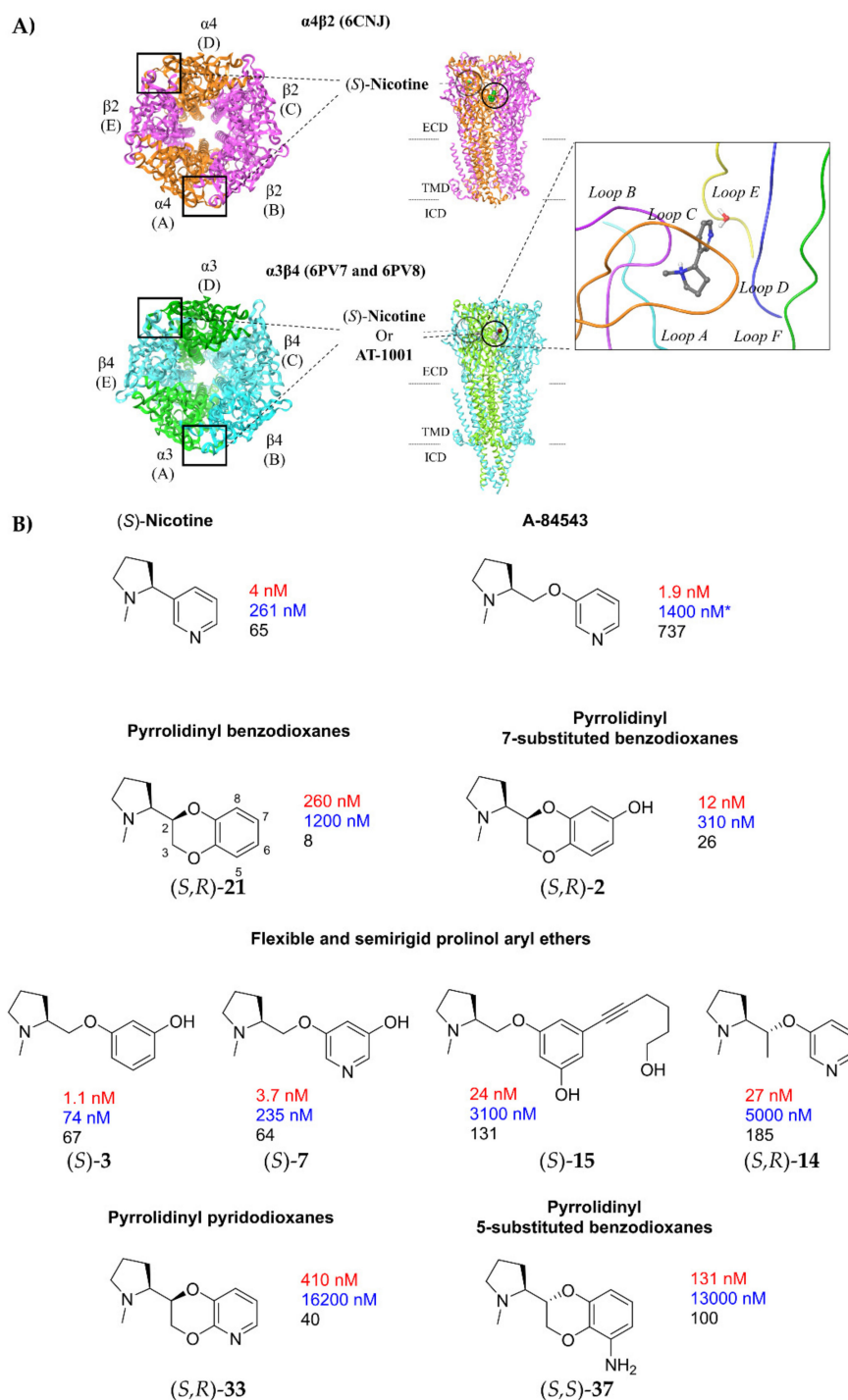


**Figure 1.** (A) Schematic overview of the  $\alpha 4\beta 2$  and  $\alpha 3\beta 4$  nAChRs architecture (adapted from 6CNJ, 6PV7, and 6PV8). The  $\alpha$ - $\beta$  localization of the orthosteric binding sites, where (S)-nicotine (6CNJ or 6PV7) and AT-1001 (6PV8) bind, are shown. Table 6. PV7, together with an overview of the loop composition of the binding site, is represented. (B) Binding affinities ( $K_i$ , nM) for rat  $\alpha 4\beta 2$  nAChR (in red) and for human  $\alpha 3\beta 4$  nAChR (in blue) and  $\alpha 4\beta 2$  vs.  $\alpha 3\beta 4$  binding selectivity (in black) of some title compounds exhibiting the highest  $\alpha 4\beta 2$  affinities. (S)-nicotine and A-84543 are reported for comparison. Asterisk on  $\alpha 3\beta 4$  affinity of A-84543 indicates that it was determined at the rat subtype.

## 2. Results and Discussion

### 2.1. Nicotine, Pyridyl Ethers of (S)-N-Me-Prolinol, and Inter-Species $\alpha4\beta2$ vs. $\alpha3\beta4$ Selectivity Ratios

#### 2.1.1. Analysis of $\alpha4\beta2$ and $\alpha3\beta4$ Affinity, Activity, and Selectivity Data from the Literature

(S)-**nicotine** (Figure 2), the most known pyrrolidine-based ligand of the nAChRs, is a competitive full agonist at all the nicotinic subtypes, with preference at the heteromeric  $\alpha2$ -6- and  $\beta2$ -4-containing subtypes rather than to homomeric  $\alpha7$  and heteromeric  $\alpha9\alpha10$  receptors. Particularly, (S)-**nicotine** is a nanomolar binder at the  $\alpha4\beta2$  subtype ( $K_i = 2$  nM at human  $\alpha4\beta2$  [34],  $K_i = 4$  nM at rat brain homogenates [32], and  $K_i = 10$  nM at rat  $\alpha4\beta2$  [35]), while it only has submicromolar affinity at the  $\alpha3\beta4$  subtype ( $K_i = 261$  nM at human  $\alpha3\beta4$  [32] and  $K_i = 440$  nM at rat  $\alpha3\beta4$  [35]), with an approximate  $\alpha4\beta2$  vs.  $\alpha3\beta4$  selectivity ratio (defined as  $K_i(\alpha3\beta4)/K_i(\alpha4\beta2)$ ) of 65 times [32]. These values have been determined in [ $^3$ H]-epibatidine competition binding experiments and are in the same range of others reported in the literature [36,37].

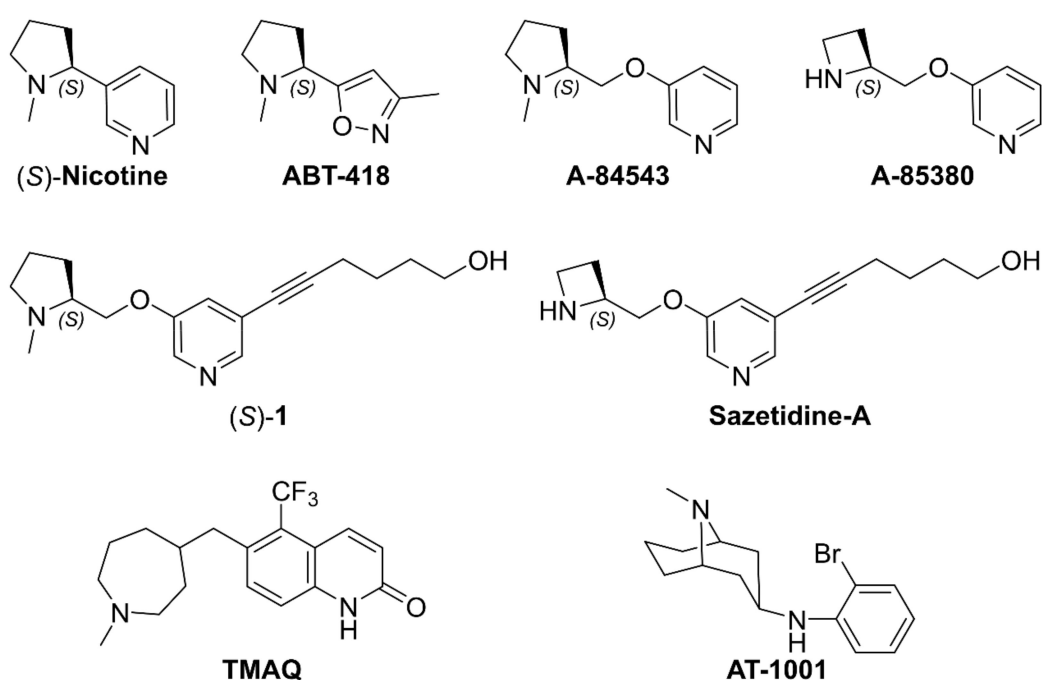


**Figure 2.** Representative structures of  $\alpha4\beta2$  and  $\alpha3\beta4$  ligands from the literature, providing useful information regarding inter-species differences of  $\alpha4\beta2$  vs.  $\alpha3\beta4$  selectivity.

At the beginning of the 1990s, the company Abbot developed and reported many pyrrolidine- and azetidine-based analogs of (S)-**nicotine**, where the pyridine ring was either replaced by other aromatic rings, such as in **ABT-418** (bioisosteric 3-methyl isoxazole, Figure 2) [38] or distanced from the alicyclic core by a methylenoxy linker. The latter approach, reported by Abreo et al. in 1996, provided a series of 3-pyridyl ethers with nano- or subnanomolar affinity for the rat  $\alpha4\beta2$  subtype in the [ $^3$ H]-(-)-cytisine displacement assay, among which compounds **A-84543** and **A-85380** (Figure 2) stood out as potent  $\alpha4\beta2$  full agonists with moderate functional selectivity over the  $\alpha3\beta4$  subtype [30]. The binding affinities at the rat  $\alpha4\beta2$  and  $\alpha3\beta4$  nAChRs in [ $^3$ H]-epibatidine competition binding experiments were later measured for **A-84543** ( $K_i = 1.9$  and 1400 nM, respectively) and for some novel 5-substituted analogs, among which (S)-**1** ( $K_i = 0.85$  and 63,000 nM, respectively, Figure 2) [39]. The resulting very high to extraordinary  $\alpha4\beta2$  vs.  $\alpha3\beta4$  selectivity ratios (737 times for **A-84543** and 74,118 times for (S)-**1**) were however referred to rat nAChRs. Inter-species variations of  $\alpha4\beta2$  vs.  $\alpha3\beta4$  selectivity were later investigated by evaluating the  $\alpha4\beta2$  and  $\alpha3\beta4$  binding affinity and selectivity ratios of **sazetidine-A** (Figure 2), an optimized derivative of (S)-**1**. Although the selectivity trends were respected, **sazetidine-A**

had a much higher  $\alpha 4\beta 2$  vs.  $\alpha 3\beta 4$  selectivity ratio at the rat subtype (24,000 times) than at the human (208 times) [40,41]. Interestingly, the difference could be ascribed to a much higher binding affinity of **sazetidine-A** at the human  $\alpha 3\beta 4$  nAChR ( $K_i = 52$  nM) compared to the rat  $\alpha 3\beta 4$  nAChR ( $K_i = 10,000$  nM). Instead, the binding affinities of **sazetidine-A** at the human  $\alpha 4\beta 2$  nAChR ( $K_i = 0.64$  nM) and at the rat  $\alpha 4\beta 2$  nAChR ( $K_i = 0.41$  nM) were almost identical.

In 2007, Young et al. identified by mutational studies two  $\alpha 3\beta 4$  amino acids (r $\beta 4$ -Ser57 and r $\beta 4$ -Ile58, corresponding to h $\beta 4$ -Asn57 and h $\beta 4$ -Val58, according to Uniprot numbering) conferring species-selectivity functional activity of **TMAQ** (Figure 2), a human  $\alpha 3\beta 4$  nAChR agonist with null activity at the rat isoform [42]. Competition binding experiments at h $\alpha 3\beta 4$  and h $\alpha 3\beta 4$  also demonstrated that these amino acids were responsible for a modest but significant (14-fold) difference in the affinity of binding of **TMAQ** to nAChRs containing the human and rat  $\alpha 4$  subunit. Similarly, in 2015, Tuan et al. reported **AT-1001** (Figure 2) as a human selective  $\alpha 3\beta 4$  nAChR ligand with similar  $K_i$ s at human and rat  $\alpha 4\beta 2$  nAChRs, while 20 times higher affinity at the human than rat  $\alpha 3\beta 4$  nAChRs [43].

### 2.1.2. Structural Rationalization of the Rat vs. Human Differences of $\alpha 4\beta 2$ vs. $\alpha 3\beta 4$ Selectivity Ratios

The much higher difference in affinity between the human  $\alpha 3\beta 4$  and the rat  $\alpha 3\beta 4$  of **sazetidine-A** compared to that of **TMAQ** and **AT-1001**, (192-times vs. 14- and 20-times), also reflected in the 115 times higher  $\alpha 4\beta 2$  vs.  $\alpha 3\beta 4$  selectivity at the rat compared to the human subtypes, prompted us to hypothesize that other structural inter-species differences of the  $\alpha 3\beta 4$  subtype could be involved. Differently, the similar binding affinities at the human and rat  $\alpha 4\beta 2$  subtypes of **sazetidine-A** and of our *in-house* ligands, among which (*S,R*)-**2**, suggest a very high degree of inter-species binding site similarity of the  $\alpha 4\beta 2$  subtype [33].

To address this question, we inspected the recently reported cryo-EM of (A) the human  $\alpha 4\beta 2$  nAChR complexed with (*S*)-**nicotine** (6CNJ) and of (B) the human  $\alpha 3\beta 4$  nAChR complexed with (*S*)-**nicotine** (6PV7), and we analyzed it together with the human/rat  $\alpha 4$ ,  $\beta 2$ ,  $\alpha 3$ , and  $\beta 4$  alignments (Figure 3). (A) At the  $\alpha 4\beta 2$  nAChR, no amino acid differences were observed between rat and human receptors within 5 Å from (*S*)-**nicotine**, explaining why the  $K_i$ s measured at the rat and human  $\alpha 4\beta 2$  are almost identical and can be considered as surrogates. (B) Instead, within 5 Å from (*S*)-**nicotine** at the human  $\alpha 3\beta 4$  subtype, the residue h $\beta 4$ -Leu121 and h $\beta 4$ -Leu112 are not conserved in the rat species, where they are replaced by r $\beta 4$ -Gln121 and r $\beta 4$ -Val112, respectively. Since the side chain of the latter (r $\beta 4$ -Val112) is not pointing at the binding site (not shown), it was not further considered. Interestingly, the residue corresponding to h $\beta 4$ -Leu121 is a Phe119 at the h $\beta 2$  subtype and has been proposed to stabilize (*S*)-**nicotine** in the h $\alpha 4\beta 2$  binding site by  $\pi$ - $\pi$  interactions with its pyridine ring. Based on these observations, we hypothesize that the residues r $\beta 4$ -Gln121, h $\beta 4$ -Leu121, and h $\beta 2$ -Phe119 are strongly affecting binding affinities (and consequently, selectivity ratios) at  $\alpha 3\beta 4$ , h $\alpha 3\beta 4$ , and h $\alpha 4\beta 2$  nAChRs, respectively.

To support our hypothesis, we performed molecular docking of the pyridyl ether **A-84543** at the h $\alpha 4\beta 2$  and h $\alpha 3\beta 4$  binding sites, extracted, aligned, and refined, respectively from the cryo-EMs 6CNJ and 6PV7. In particular, the structural water molecule known to be critical for (*S*)-**nicotine** activity at the h $\alpha 4\beta 2$  binding site and not detected in the cryo-EM, was extracted from h $\alpha 3\beta 4$  and included in the h $\alpha 4\beta 2$  binding site [20]. Additionally, we also docked **A-84543** into a model of the  $\alpha 3\beta 4$  orthosteric binding site prepared from the h $\alpha 3\beta 4$  binding site of 6PV7 by the *in silico* site directed mutagenesis of h $\beta 4$ -Leu121 into r $\beta 4$ -Gln121 (Figure 4A). In both human subtypes, **A-84543** positions the positively charged N-methyl pyrrolidine ring within the so-called aromatic box (Tyr197, Tyr204, Trp156, and Trp57 at the  $\alpha 4\beta 2$  nAChR; Tyr190, Tyr197, Trp149, and Trp59 at the  $\alpha 3\beta 4$  nAChR), with a suitable orientation of the N-methyl-pyrrolidiny ring for establishing a charge assisted H-bond with the backbone carbonyl of Trp (h $\alpha 4$ -Trp156 and h $\alpha 3$ -Trp149). Both pyridine nitrogens interact as HBAs with the structural water molecule. However, we observed a 40° plane drift between the two aromatic rings associated with a RMSD of 1.1540 Å, plausibly

since the  $\alpha 4\beta 2$ -Phe119 stabilizes the ligand through face-to-edge  $\pi$ - $\pi$  interactions, while the  $\alpha 3\beta 4$ -Leu121 can only contribute with VdW contacts. The lack of a stabilizing  $\pi$ - $\pi$  interaction causes the pyridine ring to “fall out” from the plane where the corresponding ring of (*S*)-nicotine is placed (the corresponding angle is only of  $14^\circ$ , with a RMSD of  $0.6082 \text{ \AA}$  when (*S*)-nicotine from the two original cryo-EMs are compared, Figure 3A). Additionally, the  $\alpha 3\beta 4$  binding site is less compact due to a  $2.1 \text{ \AA}$  outward displacement of loop C, which may also contribute to a lower binding affinity at the  $\alpha 3\beta 4$  and to the generally good  $\alpha 4\beta 2$  vs.  $\alpha 3\beta 4$  selectivity of pyridyl ether nicotinic ligands. Interestingly, when **A-84543** is docked at the  $\alpha 3\beta 4$ , where  $\beta 4$ -Leu121 is replaced by the more flexible and hydrophilic  $\beta 4$ -Gln121, it bends with an even wider angle of  $80^\circ$  reaching an overall RMSD of  $2.5002 \text{ \AA}$ , disallowing the conventional interactions with the binding site. These observations, taken together, could explain why pyridyl ether-based nicotinic ligands have a much higher  $\alpha 4\beta 2$  vs.  $\alpha 3\beta 4$  selectivity than  $\alpha 4\beta 2$  vs.  $\alpha 3\beta 4$  selectivity ratios.

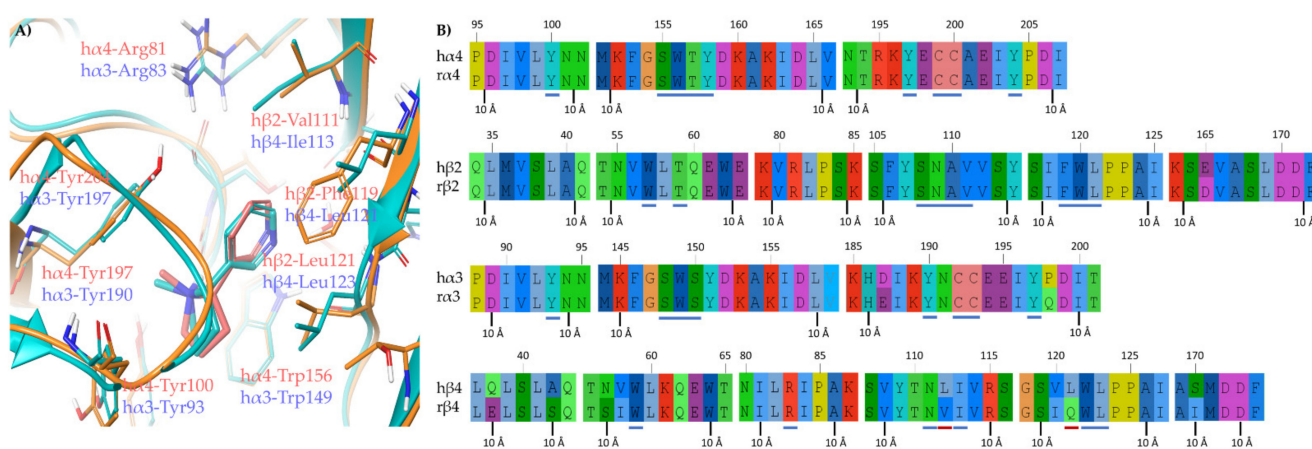


**Figure 3.** (A) Superimposition of the  $\alpha 4\beta 2$  and  $\alpha 3\beta 4$  binding sites complexed with (*S*)-nicotine (orange residues, backbone cartoons, and red ligand for  $\alpha 4\beta 2$  and light blue residues, backbone cartoons, and ligand for  $\alpha 3\beta 4$ ) extracted from the cryo-EMs 6CNJ and 6PV7, respectively. (B) Extracts of alignments of human and rat  $\alpha 4$ ,  $\beta 2$ ,  $\alpha 3$ , and  $\beta 4$ . Residues within 5 Å from the ligand has been underlined in blue, when identical between the species, in red when different.

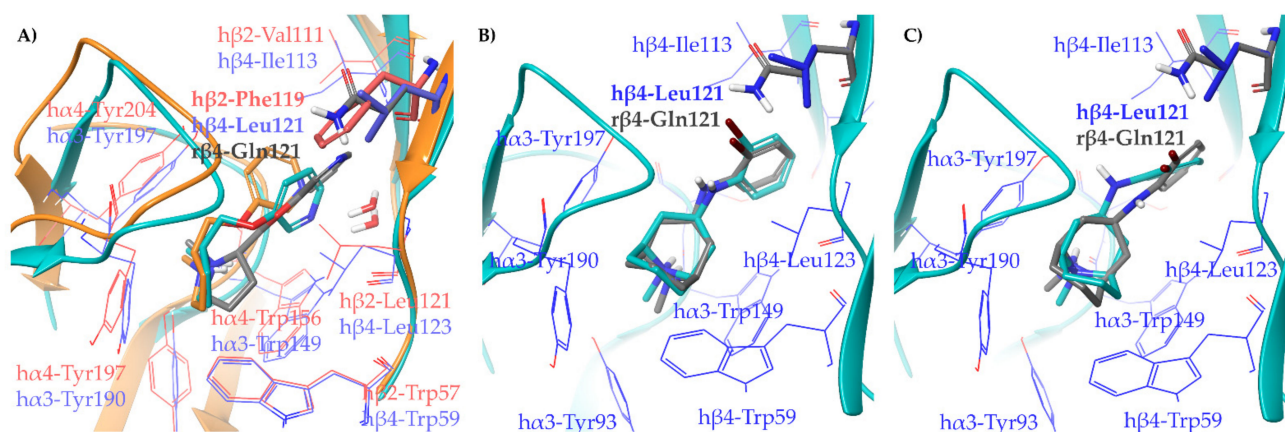


**Figure 4.** Receptor backbones are represented by orange ( $\alpha 4\beta 2$ ) or cyan ( $\alpha 3\beta 4$ ) cartoons. (A) Comparison between the proposed binding modes of **A-84543** at the  $\alpha 4\beta 2$  (PDB ID: 6CNJ, orange ligand and red residues),  $\alpha 3\beta 4$  (PDB ID: 6PV7, cyan ligand and blue residues), and at the  $\alpha 3\beta 4$  (grey ligand and residue). (B) Comparison between the original cryo-EM binding mode of **AT-1001** at the AB interface of  $\alpha 3\beta 4$  (PDB ID: 6PV8, cyan ligand and blue residues) with the docked binding pose at the  $\alpha 3\beta 4$  (grey ligand and residue) and (C) at the DE interface.

Since the cryo-EM of the complex AT-1001/ $\alpha 3\beta 4$  is also available (6PV8), and AT-1001 has been experimentally proven to bind differently at the two apparently identical  $\alpha 3\beta 4$  interfaces (AB and DE interfaces), we also prepared the  $\alpha 3\beta 4$  models based on both interfaces by in silico mutagenesis and docked AT-1001. The binding poses of AT-1001 at the  $\alpha 3\beta 4$  binding site based on the AB interface is nearly identical to that at the  $\alpha 3\beta 4$  from the cryo-EM (RMSD of 0.5936 Å). When docked at the  $\alpha 3\beta 4$  binding site based on the DE interface, the aromatic ring of AT-1001 bends inwards of around 30° (RMSD of 0.9412 Å). The less dramatic change in AT-1001 positioning, occurring at one binding interface only, could account for the lower inter-species ratios in  $\alpha 3\beta 4$  binding affinity (Figure 4B,C). An overview of the relevant interactions is reported in Table S1.

## 2.2. Rationalization of Determinants for $\alpha 4\beta 2$ vs. $\alpha 3\beta 4$ nAChR Selectivity of Small, Flexible Phenyl Ethers of (S)-N-Methyl-Prolinol

Between 2015 and 2016, Bolchi et al. reported a series of unichiral *m*-substituted phenyl ethers of (S)-N-methyl prolinol, compounds (S)-3–7, as flexible analogs of the rigid  $\alpha 4\beta 2$  partial agonist (S,R)-2, that binds the  $\alpha 4\beta 2$  nAChR with nanomolar affinity ( $K_i = 0.012 \mu\text{M}$ ) and has a moderate  $\alpha 4\beta 2$  vs.  $\alpha 3\beta 4$  selectivity ratio of 26 times (Table 1) [7,32]. Among these, (S)-3 can also be considered as the hydroxylated derivative of compound (S)-4, reported by Elliot in 1997 as a binder of  $\alpha 4\beta 2$  nAChR ( $K_i = 0.042 \mu\text{M}$ ) [44].

**Table 1.** Binding affinity data at  $\alpha 4\beta 2$  and  $\alpha 3\beta 4$  nAChRs and  $\alpha 4\beta 2$  vs.  $\alpha 3\beta 4$  selectivity ratio of compounds (S,R)-2, (S)-3–7 reported in the literature. <sup>a</sup> Tested at rat cortex using [<sup>3</sup>H]-epibatidine, unless otherwise specified. <sup>b</sup> Tested at membranes of human  $\alpha 3\beta 4$  transfected cells. <sup>c</sup> Data from Bavo et al. [33]. <sup>d</sup> Data from Bolchi et al. [32]. <sup>e</sup> Tested at whole at brain preparation using [<sup>3</sup>H]-cytisine; from Elliot et al. [44]. <sup>f</sup> Data from Bolchi et al. [7].

Compound	$\alpha 4\beta 2$ $K_i$ ( $\mu\text{M}$ ) <sup>a</sup>	$\alpha 3\beta 4$ $K_i$ ( $\mu\text{M}$ ) <sup>b</sup>	$\alpha 3\beta 4$ $K_i/\alpha 4\beta 2$ $K_i$
(S,R)-2 <sup>c</sup>	0.012	0.310	25.8
(S)-3 <sup>d</sup>	0.0011	0.074	67.3
(S)-4 <sup>e</sup>	0.042	n.a.	n.a.
(S)-5 <sup>f</sup>	0.600	4.5	7.5
(S)-6 <sup>f</sup>	0.0312	0.946	30.3
(S)-7 <sup>d</sup>	0.0037	0.235	63.5

Deconstruction of the dioxane ring of (S,R)-2 into (S)-3 switched the functional activity from  $\alpha 4\beta 2$  partial agonist to full agonist, and increased both binding affinity ( $K_i = 0.0011 \mu\text{M}$ ) and the  $\alpha 4\beta 2$  vs.  $\alpha 3\beta 4$  selectivity ratio (67-fold). Methylation of the hydroxyl group to give (S)-5 caused a sharp drop in  $\alpha 4\beta 2$  affinity ( $K_i = 0.600 \mu\text{M}$ , 400 times), while replacement with a nitro group in (S)-6 decreased affinity ( $K_i = 0.0312 \mu\text{M}$ , 28 times).

To understand the structural determinants underlying the trends in  $\alpha 4\beta 2$  affinity and  $\alpha 4\beta 2$  vs.  $\alpha 3\beta 4$  selectivity, we docked compounds (S)-3, (S)-4, (S)-5, and (S)-6 in the  $\alpha 4\beta 2$  and in the  $\alpha 3\beta 4$  binding sites, extracted and refined, respectively from the cryo-EM structures 6CNJ and 6PV7. In detail, since none of the compounds contained a pyridine nitrogen as a suitable hydrogen bond partner for the structural water molecule, and all except (S)-4 presented a substituent in the same (*meta*) position instead, we removed the water molecule from the  $\alpha 3\beta 4$  binding pocket. This approach was previously successful in describing the binding mode of (S,R)-2 at  $\alpha 4\beta 2$  and  $\alpha 3\beta 4$  nAChRs [33].

(S)-3 binds similarly at the interfaces of both subtypes and coherently overlays the pyrrolidine ring with that of (S)-nicotine and (S,R)-2 (Figure 5A). Furthermore, the

*m*-hydroxyl group of (*S*)-3 superimposes with the structural water molecule, and interacts with the backbone carbonyl of  $\beta$ 2-Asn109/ $\beta$ 4-Asn111 and the backbone NH of  $\beta$ 2-Leu121/ $\beta$ 4-Leu123 within the small and hydrophilic pocket known to be critical for nAChR affinity [33]. The 3-times higher affinity of (*S*)-3 than (*S*)-nicotine might be attributed to the replacement of a flexible water-mediated H-bond network with the more rigid and stable direct interaction between the *m*-OH and the receptor. (*S*)-3 shares the same  $\alpha$ 4 $\beta$ 2 vs.  $\alpha$ 3 $\beta$ 4 selectivity ratio than (*S*)-nicotine, and similarly to the latter, the phenolic ring of (*S*)-3 is 20° bent outwards due to the h $\beta$ 2-Phe119 to h $\beta$ 4-Leu121 replacement mentioned earlier (RMSD of 1.0536 Å).

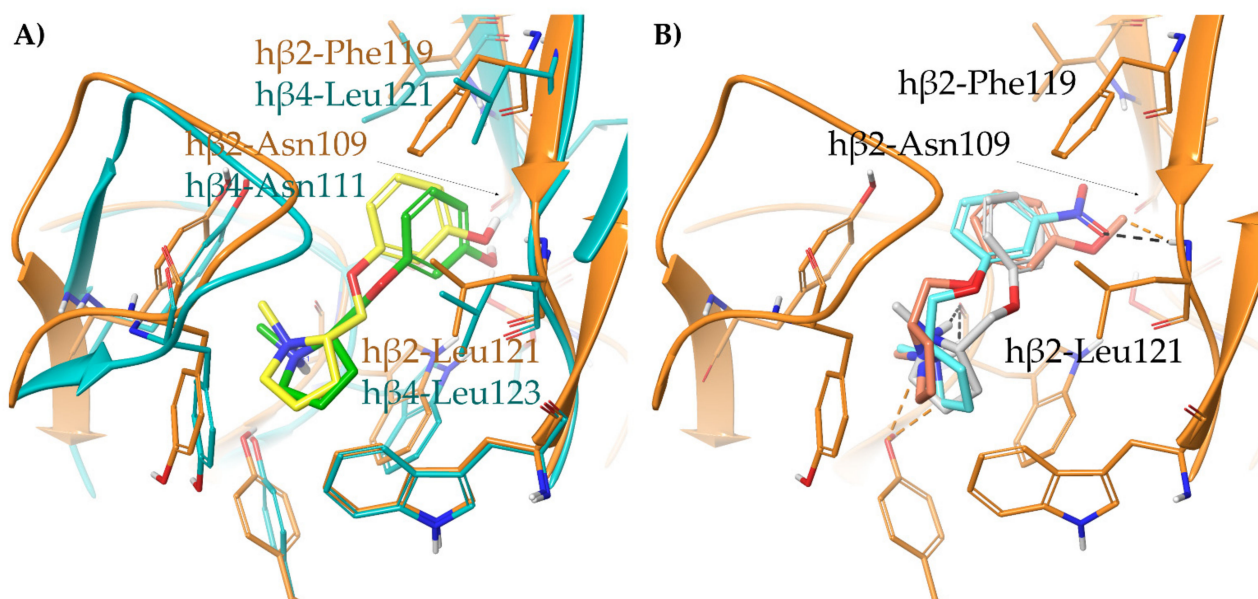


**Figure 5.** (A) Comparison of the proposed binding mode of the high affinity  $\alpha$ 4 $\beta$ 2 ligand (*S*)-3 at the h $\alpha$ 4 $\beta$ 2 (yellow ligand, orange residues and orange backbone cartoon, PDB ID: 6CNJ) and at the h $\alpha$ 3 $\beta$ 4 (green ligand, light blue residues, and light blue backbone cartoons, PDB ID: 6PV7). (B) Docking of the weak binders (*S*)-4 (light grey), (*S*)-5 (faded orange), and (*S*)-6 (cyan) at the h $\alpha$ 4 $\beta$ 2 (orange residues and orange backbone cartoon, PDB ID: 6CNJ). Unfavorable steric clashes and hydrogen bonds are depicted as dashed orange and black lines, respectively.

When the hydroxyl group of (*S*)-3 is replaced by a bulkier nitro group in (*S*)-6, the ligand is forced to assume a kinked conformation, but still interacts, although incompletely, with the backbone of  $\beta$ 2-Leu121. Instead, the less polar and bulkier methoxy group of (*S*)-5 sterically clashes with  $\beta$ 2-Leu121, while the naked (*S*)-4 lacks any feature able to reach and interact with the small hydrophilic subpocket (Figure 5B). An overview of the relevant interactions is reported in Table S2.

### 2.3. Binding Modes of the $\alpha$ 4 $\beta$ 2 Superagonist Hydroxy Pyridyl Ether of *N*-Methyl Prolinol (*S*)-7

(*S*)-7 combines in its structure the *meta*-hydroxylation of (*S*)-3 and the pyridyl ring of **A-84543**, both crucial to reach and interact with  $\beta$ 2-Asn109 and  $\beta$ 2-Leu121, either directly or by bridging a water molecule [20]. As a result, the hydroxyl pyridyl ether (*S*)-7 has nanomolar  $\alpha$ 4 $\beta$ 2 binding affinity ( $K_i = 0.0037 \mu\text{M}$ ) and a  $\alpha$ 4 $\beta$ 2 vs.  $\alpha$ 3 $\beta$ 4 selectivity ratio similar to that of (*S*)-3 (63 times) (Table 1). Whereas (*S*)-3 is a full agonist with one digit micromolar potency, (*S*)-7 is functionally an  $\alpha$ 4 $\beta$ 2 superagonist, with high efficacy (661% than the efficacy of Ach 1 mM) but low potency ( $EC_{50} = 73 \mu\text{M}$ ). Instead, it has low efficacy at the  $\alpha$ 3 $\beta$ 4 nAChR (15% than the efficacy of Ach 1 mM), and therefore is a functionally selective  $\alpha$ 4 $\beta$ 2 superagonist.

Although it is difficult to describe the functional activity at nAChRs by computational techniques only, we docked (*S*)-7 at the  $\alpha$ 4 $\beta$ 2 and  $\alpha$ 3 $\beta$ 4 binding sites to propose a plausible



binding mode and to suggest hypotheses on superagonism and functional  $\alpha 4\beta 2$  vs.  $\alpha 3\beta 4$  selectivity of (S)-7.

Due to its structural features, (S)-7 can hypothetically (A) establish hydrogen bonds with the structural water molecule through the pyridine ring or (B) replace the water molecule and directly interact through the *meta*-hydroxyl or (C) both. Therefore, we docked (S)-7 at both binding pockets, both including and removing the structural water. As expected, (S)-7 assumes two distinct binding poses at the  $\alpha 4\beta 2$  nAChR, depending on the presence or absence of water (Figure 6A). When the structural water is included, (S)-7 folds onto itself and the pyridine nitrogen interacts with water, strongly resembling the binding mode of A-84543. Instead, when the structural water is not included, (S)-7 binds with an extended conformation, similar to that of (S)-3, and places the hydroxyl group within the small hydrophilic pocket. Of particular note, when (S)-7 binds with a folded and A-84543-like conformation, the *meta*-OH establishes an hydrogen bond with  $\alpha 4$ -Tyr204. Instead, when (S)-7 binds with an extended (S)-4-like conformation, the pyridine nitrogen is placed nearby  $\alpha 4$ -Thr157, whose hydroxylated side chain is stabilized backwards by H-bond with  $\beta 2$ -Asn109. Under the assumption of receptor flexibility, we scanned the rotamers of  $\alpha 4$ -Thr157 and observed that the third most populated rotamer according to the Schrodinger rotamer library exposed the hydroxyl group at less than 4 Å from the nitrogen, suggesting the potential for hydrogen bond.

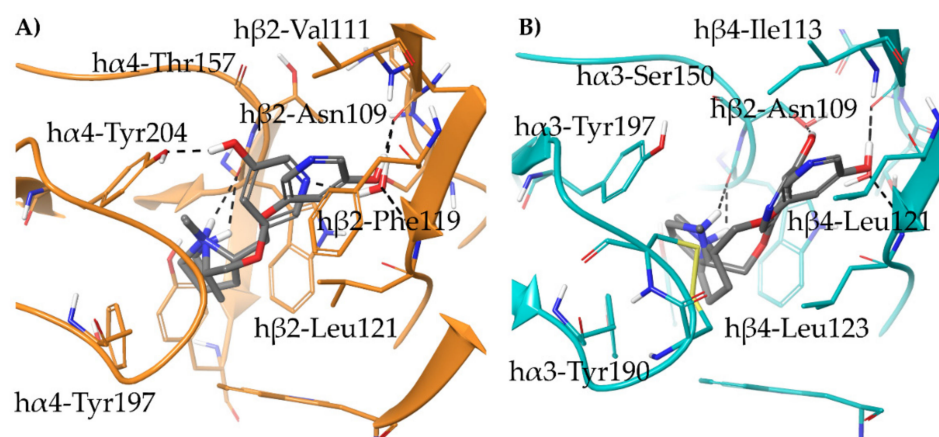


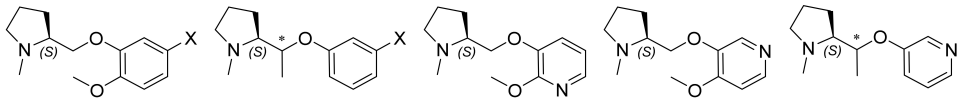
**Figure 6.** Proposed binding modes of (S)-7 (dark grey) at the (A)  $h\alpha 4\beta 2$  (PDB ID: 6CNJ) and (B) at the  $h\alpha 3\beta 4$  (PDB ID: 6PV7) binding sites, both including and removing the structural water (kinked and extended conformation, respectively). Receptor backbones are represented by orange ( $h\alpha 4\beta 2$ ) and cyan ( $h\alpha 3\beta 4$ ) cartoons. Hydrogen bonds are depicted as black dashed lines.

Although it is tempting to speculate that either the dual binding mode of (S)-7 or the additional hydrogen bonds with  $\alpha 4$ -Tyr204 or  $\alpha 4$ -Thr157 could be correlated with the superagonist activity, mutational studies would be needed to further investigate these hypotheses. At the water-free  $\alpha 3\beta 4$  nAChR, (S)-7 binds with an extended conformation similar to (S)-3 (Figure 6B). At the  $\alpha 3\beta 4$  binding site, it still folds but loses contact with the  $\beta$  subunit, interacting with  $\alpha 3$ -Ser150 instead. The similar binding pose of (S)-7 and (S)-3 at the water-free binding sites could explain the same  $\alpha 4\beta 2$  vs.  $\alpha 3\beta 4$  selectivity ratio (RMSD of 1.6933 Å), while the disruption of a critical interaction between the water-free  $\alpha 3\beta 4$  binding site and the folded conformation of (S)-7 could be correlated to the very low efficacy at this subtype, which makes (S)-7 functionally selective. An overview of the relevant interactions is reported in Table S2.

#### 2.4. Semirigid Pyrrolidine-Based Nicotinic Ligands: Rationalization of Determinants for $\alpha 4\beta 2$ nAChRs Affinity and for High $\alpha 4\beta 2$ vs. $\alpha 3\beta 4$ Selectivity of (S,R)-14

In the same work, we also reported a series of semi-rigid analogs of (S)-3, (S)-4, and A-84543, namely 8–14, where either a methyl or a methoxy group was introduced to impose conformational strains, reduce flexibility, and mimic the rigid core of the partial agonist (S,R)-2 (Table 2). Both analogs of (S)-4, ((S)-8 and (S)-10), had micromolar affinity at the  $\alpha 4\beta 2$  nAChR. The  $\alpha 4\beta 2$  affinity of compounds derived from (S)-3, ranged from 2-digits nanomolar ( $K_i = 18.9$  and  $11.1$  nM, for (S)-9 and (S,R)-11, respectively) to low submicromolar ( $K_i = 0.192$   $\mu\text{M}$  for (S,S)-11). Among the analogs of A-84543, only (S,R)-14 had nanomolar  $\alpha 4\beta 2$  affinity ( $K_i = 27$  nM).

**Table 2.** Binding affinity data at  $\alpha 4\beta 2$  and  $\alpha 3\beta 4$  nAChRs and  $\alpha 4\beta 2$  vs.  $\alpha 3\beta 4$  selectivity ratio of compounds 8–14 reported in Bolchi et al. [32]. <sup>a</sup> Tested at rat cortex using [<sup>3</sup>H]-epibatidine. <sup>b</sup> Tested at membranes of human  $\alpha 3\beta 4$  transfected cells.



Compound	$\alpha 4\beta 2$ $K_i$ ( $\mu\text{M}$ ) <sup>a</sup>	$\alpha 3\beta 4$ $K_i$ ( $\mu\text{M}$ ) <sup>b</sup>	$\alpha 3\beta 4$ $K_i/\alpha 4\beta 2$ $K_i$
(S)-8	9.4	0.749	0.08
(S)-9	0.0189	0.271	14.3
(S,R)-10	1.55	1.3	0.84
(S,R)-10 + (S,S)-10	4.59	1.4	0.31
(S,R)-11	0.011	0.257	23.4
(S,S)-11	0.192	0.752	3.9
(S)-12	7.28	0.794	0.11
(S)-13	0.255	2.1	8.2
(S,R)-14	0.027	5.0	185
(S,S)-14	0.877	5.6	6.4

All the semi-rigid compounds were docked at the  $\alpha 4\beta 2$  binding sites optimized from 6CNJ for rigid benzodioxane-based ligands as reported in Bavo et al. [33]. Lacking any feature required either displacing or interacting with the structural water molecule, (S)-8, (S,R)-10, and (S,S)-10 cannot establish any productive interaction with the  $\beta 2$  subunit (Figure 7A). Instead, (S)-9, (S,R)-11, and (S,S)-11, reflecting their nanomolar  $\alpha 4\beta 2$   $K_i$ s, directly bind the  $\beta 2$  subunit with the *m*-OH substituent (Figure 7B). Of these, (S,S)-11 shows some unfavorable steric contacts between the methyl group and the side chains of  $\beta 2$ -Leu121 and  $\alpha 4$ -Cys199, whereas the methyl substituent in (S,R)-11 and the methoxy group of (S)-9 are accommodated in a more spacious area of the binding site. Among the semi-rigid analogs of A-84543, we observed a productive orientation of the pyridyl ring only in the submicromolar binders (S)-13, (S,R)-14, and (S,S)-14, while (S)-12, with micromolar  $K_i$ , does not interact with the structural water molecule (Figure 7C). Again, whereas the methoxy and methyl substituents of (S)-13 and (S,R)-14 are accommodated in a quite spacious area, the methyl group of the weaker binder (S,S)-14 clashes with the side chain of  $\alpha 4$ -Cys199. Of utmost importance, (S,R)-14 was the most  $\alpha 4\beta 2$  selective compound of the series, with an  $\alpha 4\beta 2$  vs.  $\alpha 3\beta 4$  selectivity ratio of 185 times, while the less affinitive epimer (S,S)-14 was also not selective (6 times only). Hence, (S,R)-14 was also docked at the  $\alpha 3\beta 4$  binding site optimized from 6PV7 as reported in Bavo et al. (Figure 7D) [23]. Whereas (S,R)-14 is stabilized at the  $\alpha 4\beta 2$  nAChR by  $\pi$ - $\pi$  stacking with  $\beta 2$ -Phe119, at the  $\alpha 3\beta 4$  the pyridyl ring bends out with a wide angle of  $51^\circ$  and an overall RMSD of 2.7792 Å, losing the interaction with the structural water molecule. The same

effect was evident for (*S,R*)-**33** (discussed later), its fully rigidified analogue previously reported [5,33]. Furthermore, the binding conformation of (*S,R*)-**14** at the  $\alpha 4\beta 2$  nAChR superimposes well with that of (*S,R*)-**33**, positioning the  $\alpha$ -methyl functional group in the area where the corresponding C3 of the benzodioxane is placed (compare Figure 7D with Figure 10B). Likewise, at the  $\alpha 3\beta 4$  nAChR, the two ligands share a predicted similar conformation and binding pose, where the critical interaction between the pyridyl nitrogen and the structural water is lost, and in which the  $\alpha$ -methyl group of (*S,R*)-**14** is positioned very close to  $\alpha 3$ -Tyr197, impairing  $\alpha 3\beta 4$  binding. An overview of the relevant interactions is reported in Table S3.

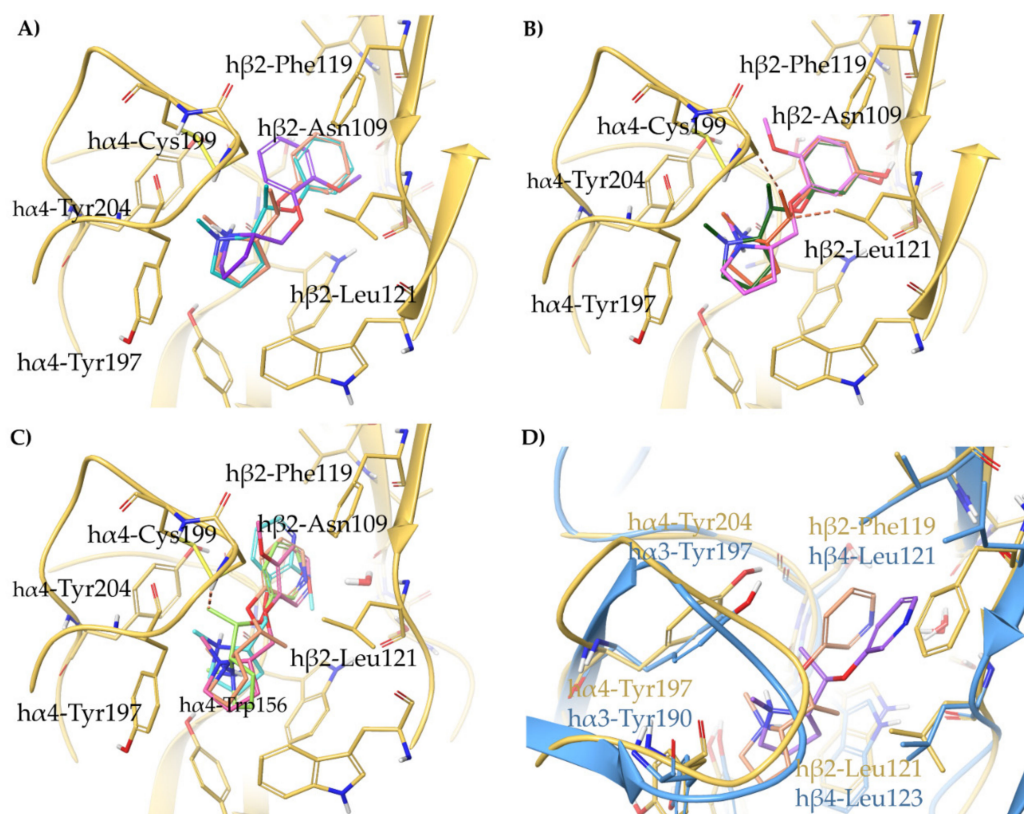


**Figure 7.** Receptor backbone and residues are depicted in yellow ( $\alpha 4\beta 2$ ) and light blue ( $\alpha 3\beta 4$ ). Unfavourable steric clashes are represented with orange dashed lines. Proposed binding modes at  $\alpha 4\beta 2$  nAChR (adapted from 6CNJ) of the (A) semirigid non-hydroxylated phenyl ethers (*S*)-**8** (purple), (*S,R*)-**10** (cyan), and (*S,S*)-**10** (faded orange); (B) semirigid hydroxylated phenyl ethers (*S*)-**9** (pink), (*S,R*)-**11** (dark green), and (*S,S*)-**11** (orange); and of (C) semirigid piridyl ethers (*S*)-**12** (light cyan), (*S*)-**13** (faded pink), (*S,R*)-**14** (faded orange), and (*S,S*)-**14** (yellow-green). (D) Comparison of the binding modes of (*S,R*)-**14** at the  $\alpha 4\beta 2$  (ligand faded orange) and at the  $\alpha 3\beta 4$  (ligand faded purple) nAChRs.

### 2.5. Structural Determinants for $\alpha 4\beta 2$ nAChR Affinity and $\alpha 4\beta 2$ vs. $\alpha 3\beta 4$ Selectivity of 5-Substituted 3-Hydrophenyl Ethers of N-Methyl Prolinol

In 2016, we developed a series of 5-substituted derivatives of (*S*)-**3** and of its analog (*S*)-**6** ((*S*)-**15**–**20**), aiming to more  $\alpha 4\beta 2$  vs.  $\alpha 3\beta 4$  selective compounds (Table 3) [7]. Coherently with the literature, compounds (*S*)-**15** and (*S*)-**18**, bearing a 6-hydroxy-1-hexynyl substituent at the 5-position, were two times more selective than (*S*)-**3** and (*S*)-**6**, respectively. Unexpectedly, the slightly shorter but still hydroxylated *p*-hydroxyphenyl moiety of (*S*)-**16** and (*S*)-**19** increased the binding affinity at the  $\alpha 3\beta 4$  nAChR than the parent compounds (*S*)-**3** (2.4 times) and (*S*)-**6** (7.7 times), causing an overall decrease of the  $\alpha 3\beta 4/\alpha 4\beta 2$  selectivity ratios.

**Table 3.** Binding affinity data at  $\alpha 4\beta 2$  and  $\alpha 3\beta 4$  nAChRs and  $\alpha 4\beta 2$  vs.  $\alpha 3\beta 4$  selectivity ratio of compounds 15–20 reported by Bolchi et al. [7]. <sup>a</sup> Tested at rat cortex using [<sup>3</sup>H]-epibatidine. <sup>b</sup> Tested at membranes of human  $\alpha 3\beta 4$  transfected cells.

Compound	$\alpha 4\beta 2$ $K_i$ ( $\mu\text{M}$ ) <sup>a</sup>	$\alpha 3\beta 4$ $K_i$ ( $\mu\text{M}$ ) <sup>b</sup>	$\alpha 3\beta 4$ $K_i/\alpha 4\beta 2$ $K_i$
(S)-15	0.0237	3.1	130.8
(S)-16	0.0038	0.030	7.9
(S)-17	0.528	0.200	0.4
(S)-18	0.0142	1.200	84.5
(S)-19	0.012	0.122	10.2
(S)-20	0.330	0.947	2.9

To interpret these data, we docked compounds (S)-15–20 to the  $\alpha 4\beta 2$  and  $\alpha 3\beta 4$  binding sites, previously adapted to the shape and size of (S)-16, the compound with the highest  $\alpha 4\beta 2$  and  $\alpha 3\beta 4$  binding affinities of the series. The results revealed a diverse binding mode at the two subtypes. At the  $\alpha 4\beta 2$  nAChR, (S)-15–16 and (S)-18–19 are stabilized by the conventional interactions: the pyrrolidine ring is placed within the aromatic box, the *m*-substituent interacts with the  $\beta$  subunit, and the aromatic ring establishes  $\pi$ - $\pi$  stacking with  $\beta 2$ -Phe119. Consequently, the *p*-hydroxyphenyl and the hexynol substituents are oriented towards the relatively small and lipophilic  $\beta 2$ -Val111, and carry the phenolic group and the hydroxyl group between  $\alpha 4$ -Glu202 and the non-conserved  $\beta 2$ -Lys79 (Figure 8A). Removal of the phenolic function to compound (S)-17 and (S)-20 deprives the two charge assisted H-bonds, and accounts for the up to 140 times loss of  $\alpha 4\beta 2$  binding.

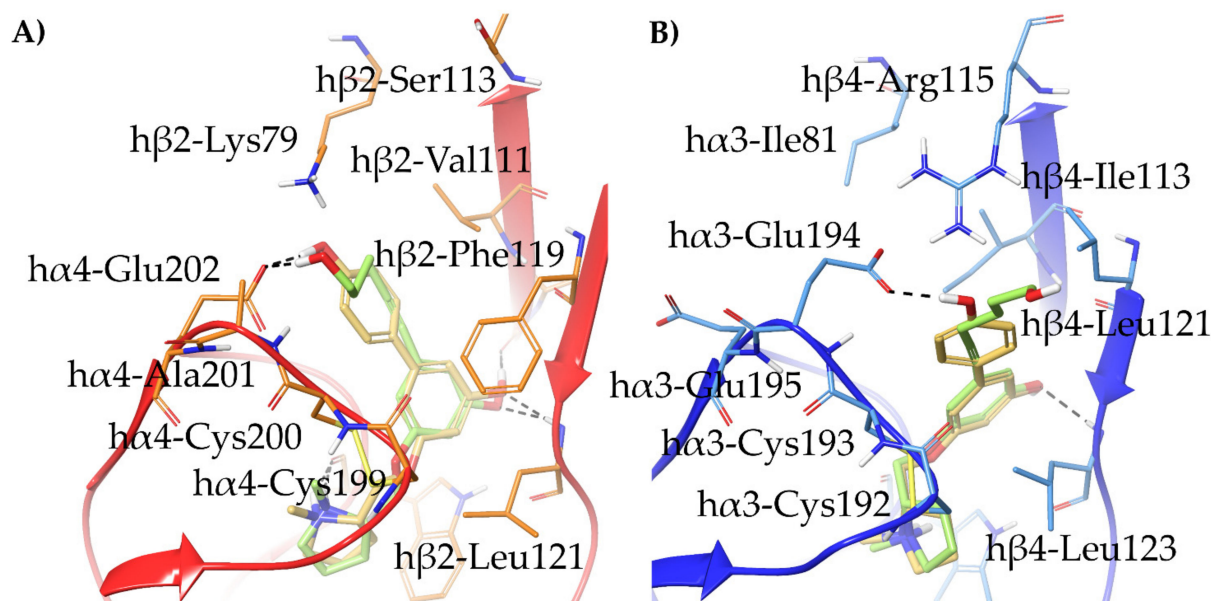


**Figure 8.** Proposed binding modes of the selective  $\alpha 4\beta 2$  ligand (S)-15 (yellow-green) and of the unselective (S)-16 (yellow) at the (A)  $\alpha 4\beta 2$  nAChR and at the (B)  $\alpha 3\beta 4$  nAChR. Receptor backbones are represented with red ( $\alpha 4\beta 2$ ) and blue ( $\alpha 3\beta 4$ ) cartoons, while  $\alpha 4\beta 2$  and  $\alpha 3\beta 4$  residues are shown in orange and light blue, respectively. Hydrogen bonds are depicted with black dashed lines.

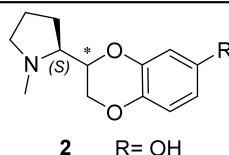
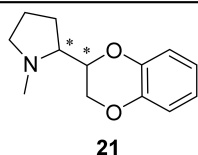
The proposed binding modes of the non-selective (*S*)-**16** and of the selective (*S*)-**15** at the  $\alpha 3\beta 4$  subtype are instead different (Figure 8B). As previously hypothesized for (*S*)-**3**, the replacement of  $\beta 2$ -Phe119 with  $\beta 4$ -Leu121 causes the phenyl moieties to bend towards  $\beta 4$ -Leu123. Additionally, the  $\alpha 4\beta 2$  residue  $\beta 2$ -Val111 is replaced by the bulkier  $\beta 4$ -Ile113, that prevents the 5-hydroxyphenyl and the 5-hexynol substituents to reach  $\alpha 3$ -Glu195 and  $\beta 4$ -Ile81, corresponding to the pair  $\alpha 4$ -Glu202/ $\beta 2$ -Lys79. As a result, the 5-*p*-hydroxyphenyl and the 5-hexynol substituents are accommodated between the disulphide bridge of  $\alpha 3$ -Cys193/Cys194 and  $\beta 4$ -Leu121. The phenolic function of (*S*)-**16** interacts with the non-conserved  $\alpha 3$ -Glu194 and  $\beta 4$ -Arg115 (corresponding to  $\alpha 4$ -Ala201 and  $\beta 2$ -Ser113, respectively) and its removal disrupts the hydrogen bond network, causing a drop in  $\alpha 3\beta 4$  affinity. On the other hand, the 5-hexynol substituent of (*S*)-**15** stretches outside from the binding pocket and looses the hydrogen bond network with  $\alpha 3$ -Glu194 and  $\beta 4$ -Arg115. An overview of the relevant interactions is reported in Table S4.

#### 2.6. Structural Determinants for $\alpha 4\beta 2$ nAChR Affinity and $\alpha 4\beta 2$ vs. $\alpha 3\beta 4$ Selectivity of 7-Substituted and Unsubstituted *N*-Methyl Pyrrolidinyl-Benzodioxanes

In 2009, we reported the synthesis of all the stereoisomers of 2-(2-pyrrolidinyl) benzodioxanes (**21**) and evaluated their binding affinities at the  $\alpha 4\beta 2$  nAChRs (Table 4) [24]. The two stereoisomers with absolute configuration “*R*” at the pyrrolidine stereocenter were devoid of affinity, while (*S,S*)-**21** and (*S,R*)-**21** had submicromolar  $\alpha 4\beta 2$   $K_i$ s of 0.47  $\mu$ M and 0.26  $\mu$ M, respectively. Later, they were shown to be micromolar binders at the  $\alpha 3\beta 4$  [5]. In 2011, we developed the series of 7-substituted analogs **2**, **22–28** (Table 4), among which only (*S,R*)-**2** was able to bind at the  $\alpha 4\beta 2$  nAChR ( $K_i = 0.012$   $\mu$ M).

**Table 4.** Binding affinity data at  $\alpha 4\beta 2$  and  $\alpha 3\beta 4$  nAChRs and  $\alpha 4\beta 2$  vs.  $\alpha 3\beta 4$  selectivity ratio of compounds **2**, **21–32**. <sup>a</sup> Tested at rat cortex using [<sup>3</sup>H]-epibatidine. <sup>b</sup> Tested at membranes of human  $\alpha 3\beta 4$  transfected cells. <sup>c</sup> Data from Pallavicini et al. [24]. <sup>d</sup> Data from Bolchi et al. [5]. <sup>e</sup> Data from Bolchi et al. [31]. <sup>f</sup> Data from Bavo et al. [33].

Compound	$\alpha 4\beta 2$ $K_i$ ( $\mu$ M) <sup>a</sup>	$\alpha 3\beta 4$ $K_i$ ( $\mu$ M) <sup>b</sup>	$\alpha 3\beta 4$ $K_i/\alpha 4\beta 2$ $K_i$
( <i>R,R</i> )- <b>21</b>	43.8 <sup>c</sup>	-	-
( <i>R,S</i> )- <b>21</b>	12.5 <sup>c</sup>	-	-
( <i>S,R</i> )- <b>21</b>	0.26 <sup>c</sup>	1.2 <sup>d</sup>	4.6
( <i>S,S</i> )- <b>21</b>	0.47 <sup>c</sup>	8.2 <sup>d</sup>	17.4
( <i>S,R</i> )- <b>2</b> <sup>e</sup>	0.012	0.310	25.8
( <i>S,S</i> )- <b>2</b> <sup>e</sup>	0.421	0.7	1.7
( <i>S,R</i> )- <b>22</b> <sup>e</sup>	42	-	-
( <i>S,R</i> )- <b>23</b> <sup>e</sup>	51	-	-
( <i>S,R</i> )- <b>24</b> <sup>e</sup>	97	-	-
( <i>S,R</i> )- <b>25</b> <sup>e</sup>	8.1	-	-
( <i>S,R</i> )- <b>26</b> <sup>e</sup>	17	-	-
( <i>S,R</i> )- <b>27</b> <sup>e</sup>	9.3	-	-
( <i>S,R</i> )- <b>28</b> <sup>e</sup>	35	-	-
( <i>S,R</i> )- <b>29</b> <sup>f</sup>	0.022	0.019	0.9
( <i>S,R</i> )- <b>30</b> <sup>f</sup>	14	4.5	0.3
( <i>S,R</i> )- <b>31</b> <sup>f</sup>	147	2.2	0.02
( <i>S,R</i> )- <b>32</b> <sup>f</sup>	6.5	1.9	0.3



<b>22</b>	R = CH <sub>3</sub>	<b>28</b>	R = Ph
<b>23</b>	R = CH <sub>2</sub> OH	<b>29</b>	R = NH <sub>2</sub>
<b>24</b>	R = COCH <sub>3</sub>	<b>30</b>	R = NO <sub>2</sub>
<b>25</b>	R = Br	<b>31</b>	R = NMe <sub>2</sub>
<b>26</b>	R = OCH <sub>3</sub>	<b>32</b>	R = NHAc
<b>27</b>	R = OCH(CH <sub>3</sub> ) <sub>2</sub>		

Our proposed binding mode at the  $\alpha 4\beta 2$  receptor for (*S,R*)-2 and for its amino analog (*S,R*)-29 (reported later, together with 30–32), easily explains the lack of affinity of any other 7-substituted analogs. The rigid and extended benzodioxane core correctly positions the 7-OH or 7-NH<sub>2</sub> group within the small hydrophilic binding pocket lined by  $\beta 2$ -Asn109 and  $\beta 2$ -Leu121, while any other bulkier group cannot be accommodated (Figure 9A). At the slightly larger binding site of the  $\alpha 3\beta 4$  nAChR, the more rigid, more extended, and better stabilized (*S,R*)-2 (RMSD of 1.3140 Å) and (*S,R*)-29 (RMSD of 1.1703 Å), are less influenced by the Phe to Leu replacement than the flexible (*S*)-3, resulting only in a moderate to null  $\alpha 4\beta 2$  vs.  $\alpha 3\beta 4$  selectivity (Figure 9B). To address the recurring  $\alpha 4\beta 2$  stereopreference for the (*S,R*) configuration, typical for both the unsubstituted and the 7-substituted analogs, we performed a conformational search of (*S,R*)-2 and (*S,S*)-2, and rigidly docked the resulting set of conformers at the  $\alpha 4\beta 2$  binding site, prepared as previously described. Although they both bind, (*S,S*)-2 binds in a high energy conformation (relative potential energy of 10.070 kJ/mol), while (*S,R*)-2 binds in the most energetically favored conformation, likely explaining the 35 times difference in binding affinity (not shown). An overview of the relevant interactions is reported in Table S5.

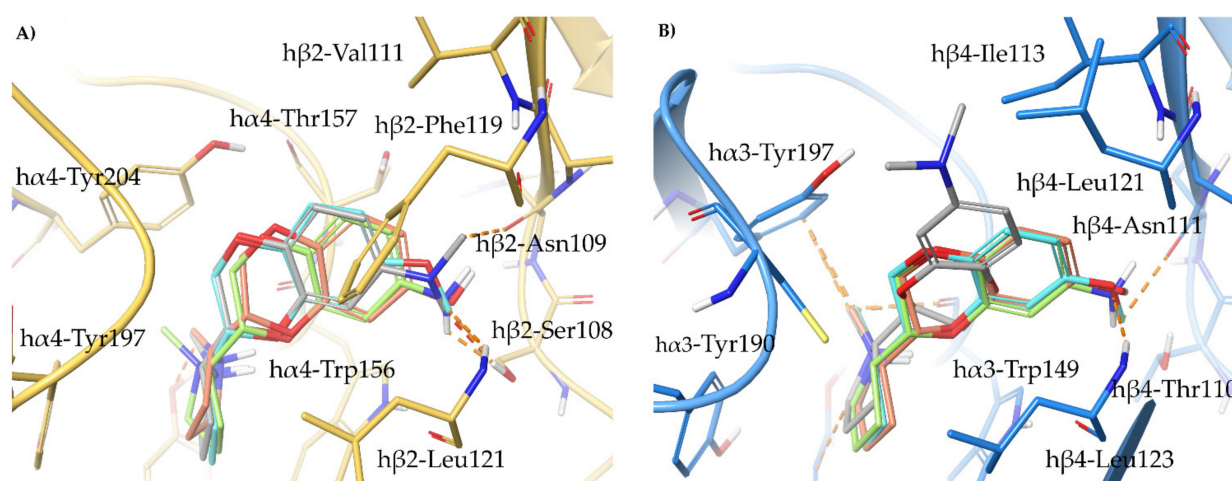


**Figure 9.** Binding poses of the high affinity ligands (*S,R*)-2 (faded orange), (*S,R*)-29 (yellow-green), and of the weak binders (*S,R*)-26 (cyan), (*S,R*)-31 (grey) at the (A)  $h\alpha 4\beta 2$  nAChR (adapted from 6CNJ, yellow residues and backbone cartoons) and at the (B)  $h\alpha 3\beta 4$  nAChR (adapted from 6PV7, light blue residues and backbone cartoons). Unfavorable and very unfavorable steric clashes are depicted with orange and red dashed lines, respectively.

### 2.7. Structural Determinants for $\alpha 4\beta 2$ nAChR Affinity and $\alpha 4\beta 2$ vs. $\alpha 3\beta 4$ Selectivity of *N*-Methylpyrrolidinyl Pyridodioxanes

In 2017, we developed 33–36, the four regioisomeric pyridodioxane-based analogs of (*S,R*)-21, in both the (*S,R*) and the (*S,S*) diastereomeric forms (Table 5) [5]. (*S,R*)-33 was the only compound retaining the submicromolar binding affinity at the  $\alpha 4\beta 2$  subtype ( $K_i = 0.41 \mu\text{M}$ ), with a 40-fold  $\alpha 4\beta 2$  vs.  $\alpha 3\beta 4$  selectivity ratio.

Relying on the proposed binding mode of (*S,R*)-33, we docked (*S,R*)-33–36 at the  $\alpha 4\beta 2$  and  $\alpha 3\beta 4$  binding sites optimized as precedently described [33]. Reflecting the binding data, only (*S,R*)-33 consistently orients the *N*-Methyl-pyrrolidine ring within the aromatic box and interacts with the structural water (Figure 10A). The low affinity of (*S,R*)-33 at  $\alpha 3\beta 4$  can be attributed to the replacement of  $\beta 2$ -Phe119 with  $\beta 4$ -Leu121, that causes the loss of a stabilizing  $\pi$ - $\pi$  interaction and the ligand to bend in the binding site (ring angle of 60.3° and RMSD of 2.1924 Å). Although this difference is observed also in the flexible ligands (described before) and in (*S,R*)-2, it is much more evident for the rigid (*S,R*)-33 and its closely related semirigid analogue (*S,R*)-14 (Figure 10B, to be compared with Figure 7D). Indeed, the rigidity of the pyridodioxane core of (*S,R*)-33 or the conformational strain imposed by the  $\alpha$ -methyl group of (*S,R*)-14, combined with the H-bond interaction with

the structural water causes the pyridodioxane and pyridyl moiety to face more tightly the  $\beta$ 2-Phe119. An overview of the relevant interactions is reported in Table S6.

**Table 5.** Binding affinity data at  $\alpha$ 4 $\beta$ 2 and  $\alpha$ 3 $\beta$ 4 nAChRs and  $\alpha$ 4 $\beta$ 2 vs.  $\alpha$ 3 $\beta$ 4 selectivity ratio of compounds 33–36, from Bolchi et al. [5]. <sup>a</sup> Tested at rat cortex using [<sup>3</sup>H]-epibatidine. <sup>b</sup> Tested at membranes of human  $\alpha$ 3 $\beta$ 4 transfected cells.

Compound	$\alpha$ 4 $\beta$ 2 K <sub>i</sub> ( $\mu$ M) <sup>a</sup>	$\alpha$ 3 $\beta$ 4 K <sub>i</sub> ( $\mu$ M) <sup>b</sup>	$\alpha$ 3 $\beta$ 4 K <sub>i</sub> / $\alpha$ 4 $\beta$ 2 K <sub>i</sub>
( <i>S,R</i> )-33	0.41	16.2	39.5
( <i>S,S</i> )-33	30.4	22	0.7
( <i>S,R</i> )-34/( <i>S,S</i> )-34	2.5	12.3	4.9
( <i>S,R</i> )-35	1.64	5.8	3.5
( <i>S,S</i> )-35	3.6	8.9	2.5
( <i>S,R</i> )-36	43	-	-
( <i>S,S</i> )-36	30	-	-

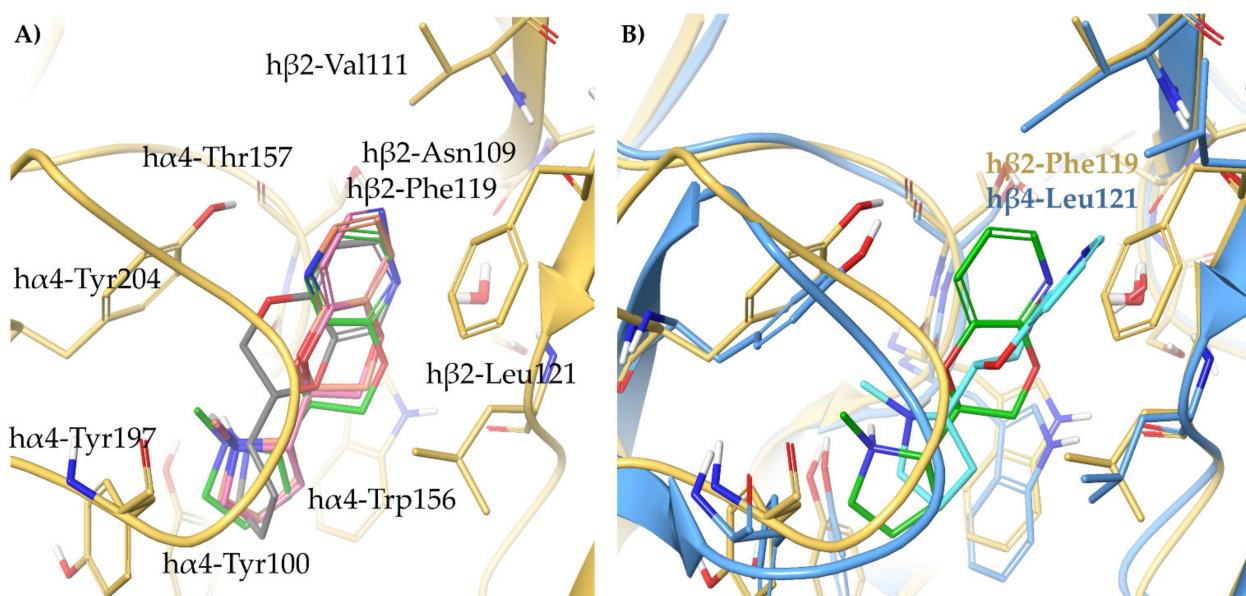


**Figure 10.** (A) Binding modes of the pyridodioxane-based selective  $\alpha$ 4 $\beta$ 2 partial agonist (*S,R*)-33 (green) and of the weak binders (*S,R*)-34 (pink), (*S,R*)-35 (grey), and (*S,R*)-36 (faded orange) at the  $\alpha$ 4 $\beta$ 2 binding site (adapted from 6CNJ, yellow residues, and yellow backbone cartoons). (B) Superimposition of (*S,R*)-33 bound at the  $\alpha$ 4 $\beta$ 2 binding site (green ligand, yellow residues, and yellow backbone cartoons, adapted from 6CNJ) and bound at  $\alpha$ 3 $\beta$ 4 binding site (cyan ligand, light blue residues, and backbone cartoons, adapted from 6PV7).

### 2.8. Structural Determinants for $\alpha$ 4 $\beta$ 2 nAChR Affinity and $\alpha$ 4 $\beta$ 2 vs. $\alpha$ 3 $\beta$ 4 Selectivity of 5- and 6-Substituted N-Methyl Pyrrolidinyl-Benzodioxanes

To complete the investigation around the benzodioxane scaffold of (*S,R*)-21, we recently developed the 5-substituted analogs 37–40 and the 6-substituted analogues 40–44 (Table 6) [33].

**Table 6.** Binding affinity data at  $\alpha 4\beta 2$  and  $\alpha 3\beta 4$  nAChRs and  $\alpha 4\beta 2$  vs.  $\alpha 3\beta 4$  selectivity ratio of compounds **37–44**, from Bavo et al. [33]. <sup>a</sup> Tested at rat cortex using [<sup>3</sup>H]-epibatidine. <sup>b</sup> Tested at membranes of human  $\alpha 3\beta 4$  transfected cells.

Compound	$\alpha 4\beta 2$ $K_i$ ( $\mu$ M) <sup>a</sup>	$\alpha 3\beta 4$ $K_i$ ( $\mu$ M) <sup>b</sup>	$\alpha 3\beta 4$ $K_i/\alpha 4\beta 2$ $K_i$
( <i>S,R</i> )- <b>37</b>	7.1	3.9	0.5
( <i>S,S</i> )- <b>37</b>	0.131	13	100
( <i>S,R</i> )- <b>38</b>	12.2	1.1	0.1
( <i>S,S</i> )- <b>38</b>	0.335	6.7	20.0
( <i>S,R</i> )- <b>39</b>	0.55	3.9	7.1
( <i>S,S</i> )- <b>39</b>	1.7	>100	>59
( <i>S,R</i> )- <b>40</b>	0.64	2.7	4.2
( <i>S,S</i> )- <b>40</b>	7.3	5.3	0.7
( <i>S,R</i> )- <b>41</b>	86	3.5	0.04
( <i>S,R</i> )- <b>42</b>	46	15	0.3
( <i>S,R</i> )- <b>43</b>	50	1.9	0.04
( <i>S,R</i> )- <b>44</b>	59	5.4	0.1

Interestingly, (*S,S*)-**37** showed high nanomolar affinity at the  $\alpha 4\beta 2$  nAChR and a very high  $\alpha 4\beta 2$  vs.  $\alpha 3\beta 4$  selectivity ratio (100 times). According to the proposed binding mode, (*S,S*)-**37** twists its benzodioxane core to fit the small hydrophilic pocket with the amino substituent, in a similar fashion to (*S,R*)-**33** (Figure 11A). The larger nature of the  $\alpha 3\beta 4$  binding site and the  $\beta 2$ -Phe119 to  $\beta 4$ -Leu121 replacement are responsible for the high  $\alpha 4\beta 2$  vs.  $\alpha 3\beta 4$  selectivity ratio of (*S,S*)-**37** (ring angle of  $232^\circ$  and RMSD of 3.1030 Å). Interestingly, the stereopreference shown for (*S,S*)-**37** (discussed previously, [33]) is not conserved among the series. Aiming at rationalizing the  $\alpha 4\beta 2$  affinity/stereochemistry patterns, we docked **37–40** at the  $\alpha 4\beta 2$  binding site (Figure 11B). (*S,S*)-**38**, but not its diastereoisomer (*S,R*)-**38**, retraces the binding mode of (*S,S*)-**37**. However, the bulky nitro group cannot fully access  $\beta 2$ -Asn109 and  $\beta 2$ -Leu121, justifying the 36-fold difference in  $\alpha 4\beta 2$  affinity. The two diastereomers of **39**, which have a similar affinity, bind very similarly, while only the diastereomer (*S,R*)-**40** correctly places the pyrrolidine ring within the aromatic box.

Although none of the 6-substituted analogs reached submicromolar  $\alpha 4\beta 2$  affinity, we found their slight preference towards the  $\alpha 3\beta 4$  subtype quite curious. Therefore, we docked them at both binding sites, and analyzed the best scored binding poses (Figure 11C,D). Apparently, the benzodioxane core of (*S,R*)-**43** is oriented similarly to that of (*S,R*)-**2**, but the 6-substituent cannot access the subpocket and stands at the entrance instead. Therefore, in the rather small and narrow  $\alpha 4\beta 2$  binding site, the ligand is pushed backwards and induces a twist of the pyrrolidine ring. Such effect is not observed when (*S,R*)-**43** is docked at the  $\alpha 3\beta 4$  binding site: The room generated by the Phe to Leu replacement and the generally more spacious cavity allow the ligand to fit in a more relaxed conformation, without any backward drift, and to place the 6-substituent in an uninfluential area of the receptor. An overview of the relevant interactions is reported in Table S5.



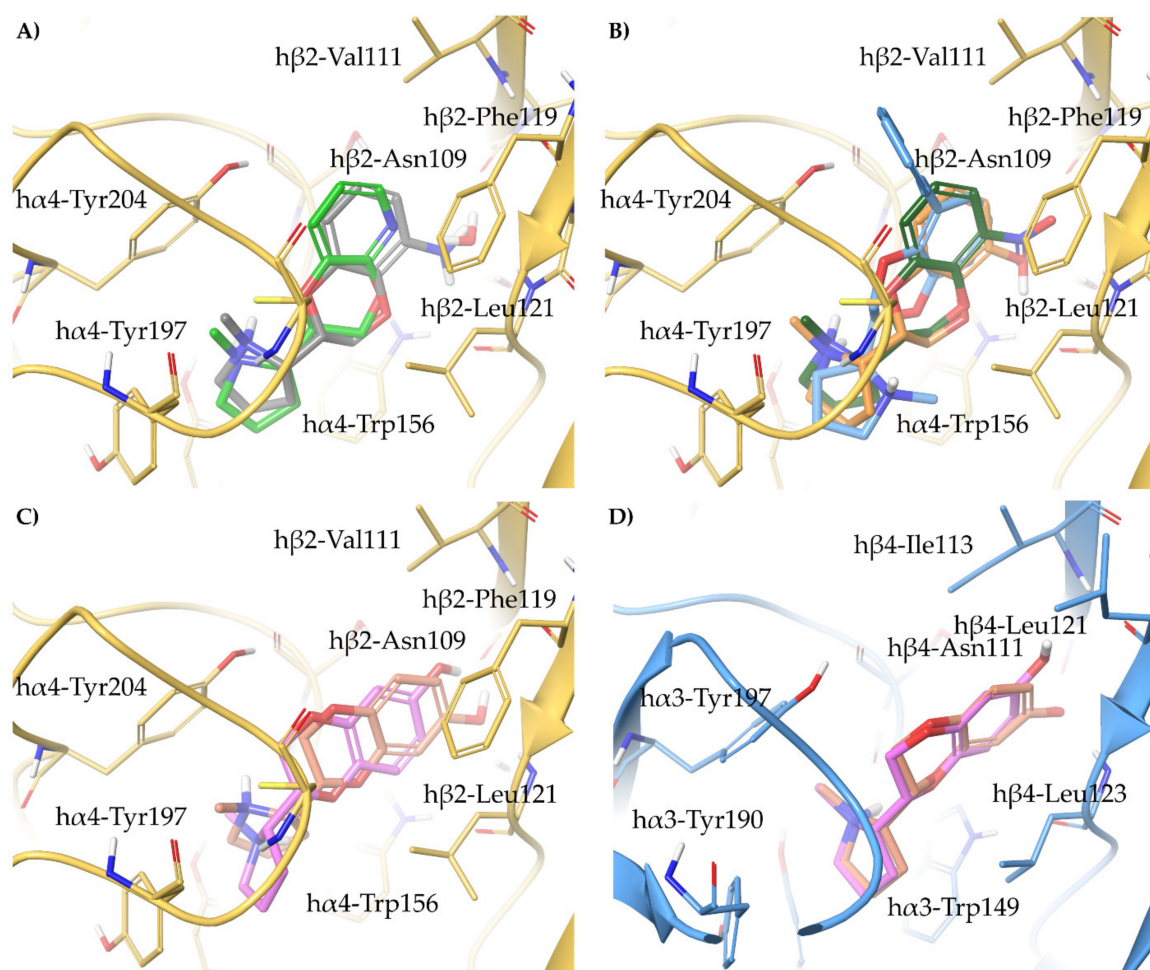


**Figure 11.** (A) Similar binding poses of (*S,R*)-33 (green) and (*S,S*)-37 (grey) at the  $h\alpha 4\beta 2$  nAChR, retraced by (B) (*S,S*)-38 (dark green) and (*S,S*)-39 (orange), but not by (*S,S*)-40 (light blue). (C) Superimposition of the binding modes of (*S,R*)-2 (faded orange) and (*S,R*)-43 (pink) at the  $h\alpha 4\beta 2$  and (D)  $h\alpha 3\beta 4$  nAChRs binding sites.

### 3. Materials and Methods

#### 3.1. Ligand Preparation

All ligands were built with the 2D editor sketch in Maestro (Schrödinger LLC: New York, NY, USA, 2019) without specifying the absolute configuration of the stereocenters [45]. Ligprep was used with default settings to assign the correct ionization state and to generate all the possible stereoisomers [46]. Of note, upon protonation of the pyrrolidine nitrogen to an asymmetric ammonium, two different absolute configurations are possible. Only ligands with “R” configuration at the nitrogen were considered, as it is the same absolute configuration of (*S*)-nicotine at the cryo-EM 6CNJ and 6PV7. Stereochemistry of all the stereocenters was visualized and the stereoisomers for which no pharmacological data were available were discarded.

#### 3.2. Binding Site Preparation: Water-Containing and Water-Free $h\alpha 4\beta 2$ and $h\alpha 3\beta 4$ from cryo-EM Structures

The  $h\alpha 4\beta 2$  and  $h\alpha 3\beta 4$  binding sites were extracted from the appropriate cryo-EM structure (6CNJ for  $h\alpha 4\beta 2$  and either 6PV7 or 6PV8  $h\alpha 3\beta 4$ ). In detail, the pair of subunits enclosing the ligand ((*S*)-nicotine in 6CNJ and 6PV7, AT-1001 in 6PV8) was extracted, truncated to preserve the extracellular domain only, and aligned. Since in 6PV8 the two interfaces (AB and DE) bind AT-1001 with different poses, they were considered separately. Water-containing binding sites were obtained as follows: The structural water molecule

bridging the pyridine nitrogen of (*S*)-**nicotine** and the  $\beta_4$  subunit, included in the  $\alpha_3\beta_4$  of 6PV7, was copied and merged with the  $\alpha_4\beta_2$  binding site. The resulting dimeric water-containing complexes were preprocessed, the hydrogen bond network optimized and subjected to constrained minimization using the Protein Preparation Wizard with default settings [47,48]. The water-containing binding sites prepared from 6CNJ and 6PV7 are hereby named for the sake of clarity 6cnj-wc- $\alpha_4\beta_2$  and 6pv7-wc- $\alpha_3\beta_4$ , respectively. Removal of the structural water molecule from the water-containing binding site provided the corresponding water-free binding sites, named 6cnj-wf- $\alpha_4\beta_2$  and 6pv7-wf- $\alpha_3\beta_4$ . The water-free binding sites originated from the two different interfaces of 6PV8 are named 6pv8-AB- $\alpha_3\beta_4$  and 6pv8-DE- $\alpha_3\beta_4$ .

### 3.3. Binding Site Preparation: Water-Containing and Water-Free $\alpha_4\beta_2$ and $\alpha_3\beta_4$ from IFD Complexes

To account for the reduced flexibility and increased size of ligands **2**, **8–14**, **21–44**, the  $\alpha_4\beta_2$  and  $\alpha_3\beta_4$  binding sites reported in Bavo et al., were employed [33]. Briefly, the most rigid and bulky compounds with the highest binding affinity at the  $\alpha_4\beta_2$  and  $\alpha_3\beta_4$  nAChRs, namely (*S,R*)-**2** and (*S,R*)-**29**, were docked at the 6cnj-wf- $\alpha_4\beta_2$  and 6pv7-wf- $\alpha_3\beta_4$ , using the Induced Fit Docking Protocol (default settings, except for scaling factor 1.0 and XP precision in the re-docking step) [49]. The resulting water-free binding sites are named 2ifd-wf- $\alpha_4\beta_2$  and 29ifd-wf- $\alpha_3\beta_4$ , respectively. Removal of the ligand and inclusion of the structural water molecule, extracted from 6PV7, provided the water-containing binding sites named 2ifd-wc- $\alpha_4\beta_2$  and 29ifd-wc- $\alpha_3\beta_4$ , respectively.

The same procedure was applied to adapt the  $\alpha_4\beta_2$  and  $\alpha_3\beta_4$  binding sites to the elongated shape of compounds (*S*)-**15–20**, by docking the ligand with the highest  $\alpha_4\beta_2$  and  $\alpha_3\beta_4$  binding affinity of the series, (*S*)-**16**, using the Induced Fit Docking Protocol [49]. The best scored  $\alpha_4\beta_2$ /*(S)*-**16** and  $\alpha_3\beta_4$ /*(S)*-**16** complexes were used for the subsequent docking steps, and named 16ifd-wf- $\alpha_4\beta_2$  and 16ifd-wf- $\alpha_3\beta_4$ .

### 3.4. Human/Rat Sequence Alignments

The primary sequences of the human and rat  $\alpha_4$ ,  $\beta_2$ ,  $\alpha_3$ , and  $\beta_4$  subunits were retrieved by Uniprot (h $\alpha_4$  P43681, r $\alpha_4$  P09483, h $\beta_2$  P17787, r $\beta_2$  P12390, h $\alpha_3$  P32297, r $\alpha_3$  P04757, h $\beta_4$  P30926, r $\beta_4$  P12392) and aligned in human-rat pairs with Clustal Omega, with default settings [50,51]. The alignments were manually inspected with Aliview [52] in the region of the binding site, defined as the area within 10 Å from the ligand (*S*)-**nicotine** in 6CNJ and 6PV7. Inter-species differences were identified within 5 Å from (*S*)-**nicotine**.

### 3.5. Binding Site Preparation: $\alpha_3\beta_4$ by In Silico Site Directed Mutagenesis

The human  $\beta_4$ -Leu121 residue of 6pv7-wc- $\alpha_3\beta_4$ , 6pv8-AB- $\alpha_3\beta_4$ , and 6pv8-DE- $\alpha_3\beta_4$  was mutated in silico into r $\beta_4$ -Gln121 and the rotamer more superimposable with the original side chain was selected (second populated rotamer not showing any steric clash), providing the binding sites named 6pv7-wc-r $\alpha_3\beta_4$ , 6pv8-AB-r $\alpha_3\beta_4$ , and 6pv8-DE-r $\alpha_3\beta_4$ .

### 3.6. Molecular Docking

Docking was performed using the Glide XP Ligand Docking Protocol docking in Maestro, Schrodinger, with default settings (van der Waals radius scaling factor: 0.8, partial cutoff: 0.15, XP precision, OPLS3e forcefield, flexible sampling), with a grid centered on the present ligand [53]. Since all the compounds presented in this work are analogues of (*S*)-**nicotine** and share with it an identical pyrrolidinyli moiety, they are expected to position it similarly to (*S*)-**nicotine**. Therefore, the highest ranked pose according to the glide model score that placed the positively charged nitrogen in the aromatic box, not further than 1.5 Å from the positively charged nitrogen of (*S*)-**nicotine**, was selected.

### 3.6.1. Docking of A-84543, (S)-nicotine, AT-1001, and Compounds 2–43

**A-84543** and (S)-nicotine were docked in the 6pv7-wc- $\alpha$ 3 $\beta$ 4 binding site, while **AT-1001** was docked in the 6pv8-AB- $\alpha$ 3 $\beta$ 4 and 6pv8-DE- $\alpha$ 3 $\beta$ 4 binding sites.

The grids generated from 6cnj-wc- $\alpha$ 4 $\beta$ 2 and 6pv7-wc- $\alpha$ 3 $\beta$ 4 were used for docking of **A-84543** and (S)-7, and those originating from 6cnj-wf- $\alpha$ 4 $\beta$ 2 and 6pv7-wf- $\alpha$ 3 $\beta$ 4 were used for docking of (S)-3–7. Compounds **2**, **8–11**, **21–32**, and **37–44** were docked at the 2ifd-wf- $\alpha$ 4 $\beta$ 2 binding site, while compounds **12–14** and **33–36** were docked in the 2ifd-wc- $\alpha$ 4 $\beta$ 2 binding site. Similarly, compounds (S,R)-**26**, (S,R)-**29**, (S,R)-**31**, (S,S)-**37**, and (S,R)-**43** were also docked at the 29ifd-wc- $\alpha$ 3 $\beta$ 4, and compounds (S,R)-**14**, (S,R)-**33**, were docked at the 29ifd-wc- $\alpha$ 4 $\beta$ 2 binding site. Compounds (S)-**15–20** were docked at the 16ifd-wf- $\alpha$ 4 $\beta$ 2 and 16ifd-wf- $\alpha$ 3 $\beta$ 4 binding sites.

Additionally, a conformational search of compounds (S,R)-**2** and (S,S)-**2** all conformers was performed using the torsional sampling (Monte Carlo Multiple Minimum) method with default settings [54]. All the resulting conformers were docked at 2ifd-wf- $\alpha$ 4 $\beta$ 2, with Glide XP as described above, but using rigid ligand sampling rather than flexible.

### 3.6.2. Self-Docking Studies

To exclude the possibility of excessive deformation of the binding pocket during the binding site preparation and to validate the docking procedure, we re-docked the native ligands in each prepared binding site using the same docking protocol used for our ligands. We considered them acceptable since the RMSD (root-mean square deviation) between the re-docked ligand and the original cryo-EM ligand was lower than 2 Å (Table S7) [55].

## 4. Conclusions

Here, we have highlighted the structural determinants for  $\alpha$ 4 $\beta$ 2 vs.  $\alpha$ 3 $\beta$ 4 subtype selectivity in a large series of flexible, semi-rigid, and rigid analogues of the  $\alpha$ 4 $\beta$ 2 vs.  $\alpha$ 3 $\beta$ 4 selective prolinol pyridyl ether **A-84543** by docking at the binding sites of the two human nicotinic subtypes, whose structures have been recently determined by cryo-electron microscopy.

Our analysis was necessarily based on the comparison of  $\alpha$ 4 $\beta$ 2 with  $\alpha$ 3 $\beta$ 4 binding affinities. While the  $\alpha$ 4 $\beta$ 2 affinities of the title compounds are similar in rat and in man [33], the  $\alpha$ 3 $\beta$ 4 affinities are generally much lower in rat than in man resulting in much higher  $\alpha$ 4 $\beta$ 2 vs.  $\alpha$ 3 $\beta$ 4 selectivity when the terms of comparison is the  $\alpha$ 3 $\beta$ 4 affinity rather than the relatively higher  $\alpha$ 4 $\beta$ 2 affinity. In this regard, the pyridyl ether **Sazetidine-A** is a case in point. Consequently, whereas the use of human  $\alpha$ 4 $\beta$ 2 structures for docking is acceptable in any case, docking cannot be regardless of the use of human or rat  $\alpha$ 3 $\beta$ 4 structure. To explain such a different behaviour, we evaluated the role, for the  $\alpha$ 3 $\beta$ 4 affinity of **A-84543**, of the not-inter-species conserved position 121 in the  $\beta$ 4 side (r $\beta$ 4-Gln121  $\rightarrow$  h $\beta$ 4-Leu121). This position seems to be crucial for the  $\alpha$ 4 $\beta$ 2 vs.  $\alpha$ 3 $\beta$ 4 subtype selectivity since it corresponds, in the h $\beta$ 2 side, to Phe119, which is advantageously involved in a  $\pi$ - $\pi$ stabilization with the pyridine ring. Well, we observed that the polar and flexible amino acid r $\beta$ 4-Gln121 disfavoured the interaction of the **A-84543** pyridine ring with the  $\beta$ 4 side even more than the rigid and lipophilic h $\beta$ 4-Leu121, due to the reduced lipophilic VdW contacts and excessive flexibility, possibly explaining the high (about a hundred times), but not exceptional  $\alpha$ 4 $\beta$ 2 vs. human- $\alpha$ 3 $\beta$ 4 selectivity of the pyridyl ether **Sazetidine-A** and of our most selective compounds.

Based on these premises, a systematic docking analysis of the **A-84543** analogues was conducted into the cryo-EM structures of the two human subtypes drawing the following conclusions about the  $\alpha$ 4 $\beta$ 2 affinity and the over  $\alpha$ 3 $\beta$ 4 selectivity of the lead compounds reported in Figure 1.

- **A-84543** and (S)-nicotine interact with the so-called aromatic box through the pyrrolidine N<sup>+</sup> in both subtypes and with  $\beta$ 2-Phe119 through the pyridine ring. In the  $\alpha$ 3 $\beta$ 4 binding site, due to the absence of phenylalanine in the  $\beta$ 4 side, the pyridine of the flexible **A-84543** “falls out” from the plane occupied in the  $\alpha$ 4 $\beta$ 2 binding site

whereas the nicotine pyridine maintains a substantially unchanged disposition. This is consistent with the high selectivity of **A-84543** and the only moderate one of nicotine.

- The docking of the 3-hydroxy phenyl ether (*S*)-**3** is very similar to that of (*S*)-**nicotine**: Overlap of the pyrrolidine rings, same interactions with the  $\beta$ 2 hydrophilic sub-pocket through the *m*-OH rather than structural water and same minimal change of the disposition of the aromatic ring in the two subtypes. This is consistent with the only moderate selectivity displayed by both compounds.
- For the hydroxypyridyl ether (*S*)-**7**,  $\alpha$ 4 $\beta$ 2 super-agonist with almost null  $\alpha$ 3 $\beta$ 4 activity but with an affinity and selectivity profiles very similar to those of nicotine, a hydroxyphenyl ether-like extended pose without water-mediated interaction and an **A-83543**-like folded pose with pyridine nitrogen interacting with structural water can be assumed in both subtypes. Such a dualism could be correlated with the significantly different degree of selectivity, typical of this compound, in binding and functional tests.
- The 3,5-disubstituted phenyl ethers show the conventional  $\alpha$ 4 $\beta$ 2 interactions (N<sup>+</sup>-aromatic box, phenyl-  $\beta$ 2-Phe119) and, in the case of the 3-hydroxy-5-(6-hydroxyhexinyl) phenyl ether (*S*)-**15**, an additional interaction of the chain's terminal OH with an  $\alpha$ 4 glutamic acid residue. Such interaction with the corresponding identical  $\alpha$ 3 aminoacidic residue is lost in the  $\alpha$ 3 $\beta$ 4 binding site. This is consistent with the high selectivity (131 times) of the above derivative.
- The (*S,R*) diastereomer of the pyrrolidinyl pyridodioxane with N in place of benzodioxane C(5)H ((*S,R*)-**33**) accommodates its N<sup>+</sup> in the aromatic box of the  $\alpha$ 4 $\beta$ 2 binding site and establishes a pyridine- $\beta$ 2-Phe119 interaction and a water-mediated interaction with the hydrophilic  $\beta$ 2 sub-pocket through the pyridine nitrogen. These two interactions are lost when the molecule is docked into the  $\alpha$ 3 $\beta$ 4 binding site. Such binding modes are conserved and favoured in (*S,R*)-**14**, where pyridodioxane deconstruction to  $\alpha$ -methyl prolinol pyridyl ether corresponds to a significant increase in  $\alpha$ 4 $\beta$ 2 affinity (410 nM  $\rightarrow$  27 nM) and selectivity (40  $\rightarrow$  185 times).
- The high  $\alpha$ 4 $\beta$ 2 affinity of 7-OH and 7-NH<sub>2</sub> substituted pyrrolidinyl benzodioxanes (*S,R*)-**2** and (*S,R*)-**29** is traceable to that of the prolinol 3-hydroxyphenyl ether (*S*)-**3**, without involvement of structural water. On the other hand, the significantly lower or null selectivity could be ascribed to a less detrimental effect of Phe to Leu replacement for the rigid and extended benzodioxane scaffold compared with flexible aryloxymethyl residues.
- With opposite stereo-preference concerning the dioxane stereocenter, the 5-amino substitution at benzodioxane ((*S,S*)-**37**) maintains high  $\alpha$ 4 $\beta$ 2 affinity thanks to the same productive interactions established by the above mentioned 7-substituted pyrrolidinyl benzodioxanes, but, notably, it does not confer the ability to interact with the wider  $\beta$ 4 minus side resulting in high selectivity.

In a nutshell, comparative docking into the two human  $\alpha$ 4 $\beta$ 2 and  $\alpha$ 3 $\beta$ 4 nAChR structures of this large series of pyrrolidine based  $\alpha$ 4 $\beta$ 2 ligands indicates that constantly discriminating factors for the  $\alpha$ 4 $\beta$ 2 vs.  $\alpha$ 3 $\beta$ 4 subtype selectivity are the stabilization of the ligand's aromatic ring by the not conserved  $\beta$ 2-Phe119 residue and direct or water mediated interaction with hydrophilic residues of the  $\beta$  minus side conditioned by decoration of the aromatic ring and extensibility of the substructure of which it is part (Figure 12). The remarkable subtype selectivity achieved by some derivatives, such as the 5-amino substituted pyrrolidinyl benzodioxane (*S,S*)-**37**, the semirigid  $\alpha$ -methyl prolinol pyridyl ether (*S,R*)-**14**, and the hydroxyhexinyl phenol derivative (*S*)-**15**, suggests that such discrimination can be highly effective.

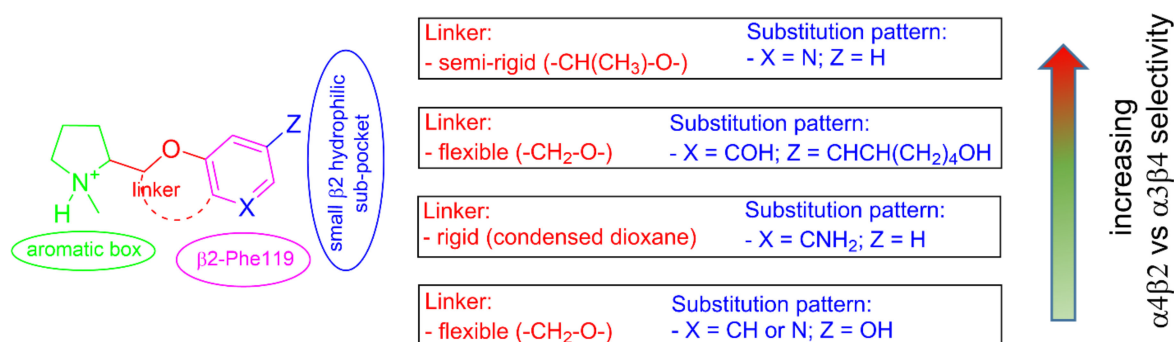


**Figure 12.** Crucial observations regarding  $\alpha 4\beta 2$  vs.  $\alpha 3\beta 4$  selectivity.

**Supplementary Materials:** Table S1: Overview of the relevant interactions of the compounds (S)-nicotine, A-84543, and AT-1001 reported in Figure 4; Table S2: Overview of the relevant interactions of the compounds (S)-3–7 reported in Figures 5 and 6; Table S3: Overview of the relevant interactions of the compounds (S)-8–14 reported in Figure 7; Table S4: Overview of the relevant interactions of the compounds (S)-15 and (S)-16 reported in Figure 8; Table S5: Overview of the relevant interactions of the compounds (S,R)-2, (S,R)-26, (S,R)-29, (S,R)-31, and (S,S)-37–40 reported in Figures 9 and 11, respectively; Table S6: Overview of the relevant interactions of the compounds (S,R)-33–36 reported in Figure 10; Table S7: RMSD values from the self-docking study.

**Author Contributions:** Conceptualization, F.B. and C.B.; methodology, F.B. and R.A.; software, F.B. and R.A.; formal analysis, F.B. and R.A.; investigation, F.B. and R.A.; writing—original draft preparation, F.B. and M.P.; writing—review and editing, F.B., M.P. and C.B.; supervision, C.B.; project administration, C.B. All authors have read and agreed to the published version of the manuscript.

**Funding:** This research received no external funding.

**Institutional Review Board Statement:** Not applicable.

**Informed Consent Statement:** Not applicable.

**Data Availability Statement:** Data presented in this study are available on request from the corresponding author.

**Conflicts of Interest:** The authors declare no conflict of interest.

**Sample Availability:** Samples of the compounds 2–44 are available from the authors.

## References

- Terry, A.V., Jr.; Callahan, P.M. Nicotinic acetylcholine receptor ligands, cognitive function, and preclinical approaches to drug discovery. *Nicotine Tob. Res.* **2018**, *21*, 383–394. [[CrossRef](#)]
- Yu, L.-F.; Zhang, H.-K.; Caldarone, B.J.; Eaton, J.B.; Lukas, R.J.; Kozikowski, A.P. Recent developments in novel antidepressants targeting  $\alpha 4\beta 2$ -nicotinic acetylcholine receptors. *J. Med. Chem.* **2014**, *57*, 8204–8223. [[CrossRef](#)] [[PubMed](#)]
- Wang, J.; Lindstrom, J. Orthosteric and allosteric potentiation of heteromeric neuronal nicotinic acetylcholine receptors. *Br. J. Pharmacol.* **2018**, *175*, 1805–1821. [[CrossRef](#)] [[PubMed](#)]
- Rahman, S.; Engleman, E.A.; Bell, R.L. Nicotinic receptor modulation to treat alcohol and drug dependence. *Front. Neurosci.* **2015**, *8*, 426. [[CrossRef](#)]
- Bolchi, C.; Bavo, F.; Gotti, C.; Fumagalli, L.; Fasoli, F.; Binda, M.; Mucchiello, V.; Sciacaluga, M.; Plutino, S.; Fucile, S.; et al. From pyrrolidinyl-benzodioxane to pyrrolidinyl-pyridodioxanes, or from unselective antagonism to selective partial agonism at  $\alpha 4\beta 2$  nicotinic acetylcholine receptor. *Eur. J. Med. Chem.* **2017**, *125*, 1132–1144. [[CrossRef](#)]
- Rego Campello, H.; Del Villar, S.G.; Honraedt, A.; Minguez, T.; Oliveira, A.S.F.; Ranaghan, K.E.; Shoemark, D.K.; Bermudez, I.; Gotti, C.; Sessions, R.B.; et al. Unlocking nicotinic selectivity via direct C-H functionalization of (–)-cytisine. *Chem* **2018**, *4*, 1710–1725. [[CrossRef](#)]
- Bolchi, C.; Bavo, F.; Fumagalli, L.; Gotti, C.; Fasoli, F.; Moretti, M.; Pallavicini, M. Novel 5-substituted 3-hydroxyphenyl and 3-nitrophenyl ethers of S-prolinol as  $\alpha 4\beta 2$ -nicotinic acetylcholine receptor ligands. *Bioorg. Med. Chem. Lett.* **2016**, *26*, 5613–5617. [[CrossRef](#)]
- Bavo, F.; Pucci, S.; Fasoli, F.; Lammi, C.; Moretti, M.; Mucchiello, V.; Lattuada, D.; Viani, P.; De Palma, C.; Budriesi, R.; et al. Potent antiglioblastoma agents by hybridizing the onium-alkyloxy-stilbene based structures of an  $\alpha 7$ -nAChR,  $\alpha 9$ -nAChR antagonist and of a pro-oxidant mitocan. *J. Med. Chem.* **2018**, *61*, 10531–10544. [[CrossRef](#)] [[PubMed](#)]

9. Walsh, R.M.; Roh, S.-H.; Gharpure, A.; Morales-Perez, C.L.; Teng, J.; Hibbs, R.E. Structural principles of distinct assemblies of the human  $\alpha 4\beta 2$  nicotinic receptor. *Nature* **2018**, *557*, 261–265. [[CrossRef](#)]
10. Gharpure, A.; Teng, J.; Zhuang, Y.; Noviello, C.M.; Walsh, R.M., Jr.; Cabuco, R.; Howard, R.J.; Zaveri, N.T.; Lindahl, E.; Hibbs, R.E. Agonist selectivity and ion permeation in the  $\alpha 3\beta 4$  ganglionic nicotinic receptor. *Neuron* **2019**, *104*, 501–511. [[CrossRef](#)]
11. Flores, C.M.; DeCamp, R.M.; Kilo, S.; Rogers, S.W.; Hargreaves, K.M. Neuronal nicotinic receptor expression in sensory neurons of the rat trigeminal ganglion: Demonstration of  $\alpha 3\beta 4$ , a novel subtype in the mammalian nervous system. *J. Neurosci.* **1996**, *16*, 7892–7901. [[CrossRef](#)] [[PubMed](#)]
12. McBride, P.E. The health consequences of smoking: Cardiovascular diseases. *Med. Clin. N. Am.* **1992**, *76*, 333–353. [[CrossRef](#)]
13. Stolerman, I.P.; Garcha, H.S.; Mirza, N.R. Dissociations between the locomotor stimulant and depressant effects of nicotinic agonists in rats. *Psychopharmacology* **1995**, *117*, 430–437. [[CrossRef](#)]
14. Antolin-Fontes, B.; Ables, J.L.; Görlich, A.; Ibañez-Tallon, I. The habenulo-interpeduncular pathway in nicotine aversion and withdrawal. *Neuropharmacology* **2015**, *96*, 213–222. [[CrossRef](#)]
15. Jackson, K.J.; Muldoon, P.P.; De Biasi, M.; Damaj, M.I. New mechanisms and perspectives in nicotine withdrawal. *Neuropharmacology* **2015**, *96*, 223–234. [[CrossRef](#)]
16. Saladino, A.C.; Xu, Y.; Tang, P. Homology Modeling and Molecular Dynamics Simulations of Transmembrane Domain Structure of Human Neuronal Nicotinic Acetylcholine Receptor. *Biophys. J.* **2005**, *88*, 1009–1017. [[CrossRef](#)]
17. Pedretti, A.; Marconi, C.; Bolchi, C.; Fumagalli, L.; Ferrara, R.; Pallavicini, M.; Valoti, E.; Vistoli, G. Modelling of full-length human  $\alpha 4\beta 2$  nicotinic receptor by fragmental approach and analysis of its binding modes. *Biochem. Biophys. Res. Commun.* **2008**, *369*, 648–653. [[CrossRef](#)] [[PubMed](#)]
18. Morales-Perez, C.L.; Noviello, C.M.; Hibbs, R.E. X-ray structure of the human  $\alpha 4\beta 2$  nicotinic receptor. *Nature* **2016**, *538*, 411–415. [[CrossRef](#)] [[PubMed](#)]
19. Harpsøe, K.; Hald, H.; Timmermann, D.B.; Jensen, M.L.; Dyhring, T.; Nielsen, E.Ø.; Peters, D.; Balle, T.; Gajhede, M.; Kastrup, J.S.; et al. Molecular Determinants of Subtype-selective Efficacies of Cytisine and the Novel Compound NS3861 at Heteromeric Nicotinic Acetylcholine Receptors. *J. Biol. Chem.* **2013**, *288*, 2559–2570. [[CrossRef](#)]
20. Blum, A.P.; Lester, H.A.; Dougherty, D.A. Nicotinic pharmacophore: The pyridine N of nicotine and carbonyl of acetylcholine hydrogen bond across a subunit interface to a backbone NH. *Proc. Natl. Acad. Sci. USA* **2010**, *107*, 13206–13211. [[CrossRef](#)] [[PubMed](#)]
21. Celie, P.H.N.; van Rossum-Fikkert, S.E.; van Dijk, W.J.; Brejc, K.; Smit, A.B.; Sixma, T.K. Nicotine and carbamylcholine binding to nicotinic acetylcholine receptors as studied in AChBP crystal structures. *Neuron* **2004**, *41*, 907–914. [[CrossRef](#)]
22. Braida, D.; Ponzoni, L.; Moretti, M.; Viani, P.; Pallavicini, M.; Bolchi, C.; Appiani, R.; Bavo, F.; Gotti, C.; Sala, M. Behavioural and pharmacological profiles of zebrafish administrated pyrrolidiny benzodioxanes and prolinol aryl ethers with high affinity for heteromeric nicotinic acetylcholine receptors. *Psychopharmacology* **2020**, *237*, 2317–2326. [[CrossRef](#)]
23. Pallavicini, M.; Moroni, B.; Bolchi, C.; Cilia, A.; Clementi, F.; Fumagalli, L.; Gotti, C.; Meneghetti, F.; Riganti, L.; Vistoli, G.; et al. Synthesis and  $\alpha 4\beta 2$  nicotinic affinity of unichiral 5-(2-pyrrolidiny) oxazolidinones and 2-(2-pyrrolidiny) benzodioxanes. *Bioorg. Med. Chem. Lett.* **2006**, *16*, 5610–5615. [[CrossRef](#)] [[PubMed](#)]
24. Pallavicini, M.; Bolchi, C.; Binda, M.; Cilia, A.; Clementi, F.; Ferrara, R.; Fumagalli, L.; Gotti, C.; Moretti, M.; Pedretti, A.; et al. 5-(2-Pyrrolidiny) oxazolidinones and 2-(2-pyrrolidiny) benzodioxanes: Synthesis of all the stereoisomers and  $\alpha 4\beta 2$  nicotinic affinity. *Bioorg. Med. Chem. Lett.* **2009**, *19*, 854–859. [[CrossRef](#)]
25. Bolchi, C.; Bavo, F.; Appiani, R.; Roda, G.; Pallavicini, M. 1,4-Benzodioxane, an evergreen, versatile scaffold in medicinal chemistry: A review of its recent applications in drug design. *Eur. J. Med. Chem.* **2020**, *200*, 112419. [[CrossRef](#)] [[PubMed](#)]
26. Straniero, V.; Pallavicini, M.; Chiodini, G.; Ruggeri, P.; Fumagalli, L.; Bolchi, C.; Corsini, A.; Ferri, N.; Ricci, C.; Valoti, E. Farnesyltransferase inhibitors: CAAX mimetics based on different biaryl scaffolds. *Bioorg. Med. Chem. Lett.* **2014**, *24*, 2924–2927. [[CrossRef](#)]
27. Straniero, V.; Pallavicini, M.; Chiodini, G.; Zanutto, C.; Volontè, L.; Radaelli, A.; Bolchi, C.; Fumagalli, L.; Sanguinetti, M.; Menchinelli, G.; et al. 3-(Benzodioxan-2-ylmethoxy)-2,6-difluorobenzamides bearing hydrophobic substituents at the 7-position of the benzodioxane nucleus potently inhibit methicillin-resistant Sa and Mtb cell division. *Eur. J. Med. Chem.* **2016**, *120*, 227–243. [[CrossRef](#)]
28. Fumagalli, L.; Pallavicini, M.; Budriesi, R.; Gobbi, M.; Straniero, V.; Zagami, M.; Chiodini, G.; Bolchi, C.; Chiarini, A.; Micucci, M.; et al. Affinity and activity profiling of unichiral 8-substituted 1,4-benzodioxane analogues of WB4101 reveals a potent and selective  $\alpha 1\beta$ -adrenoceptor antagonist. *Eur. J. Med. Chem.* **2012**, *58*, 184–191. [[CrossRef](#)]
29. Bolchi, C.; Valoti, E.; Straniero, V.; Ruggeri, P.; Pallavicini, M. From 2-aminomethyl-1,4-benzodioxane enantiomers to unichiral 2-cyano- and 2-carbonyl-substituted benzodioxanes via dichloroamine. *J. Org. Chem.* **2014**, *79*, 6732–6737. [[CrossRef](#)]
30. Abreo, M.A.; Lin, N.-H.; Garvey, D.S.; Gunn, D.E.; Hettinger, A.-M.; Wasicak, J.T.; Pavlik, P.A.; Martin, Y.C.; Donnelly-Roberts, D.L.; Anderson, D.J.; et al. Novel 3-pyridyl ethers with subnanomolar affinity for central neuronal nicotinic acetylcholine receptors. *J. Med. Chem.* **1996**, *39*, 817–825. [[CrossRef](#)]
31. Bolchi, C.; Gotti, C.; Binda, M.; Fumagalli, L.; Pucci, L.; Pistillo, F.; Vistoli, G.; Valoti, E.; Pallavicini, M. Unichiral 2-(2'-pyrrolidiny)-1,4-benzodioxanes: The 2R,2'S diastereomer of the N-methyl-7-hydroxy analogue is a potent  $\alpha 4\beta 2$ - and  $\alpha 6\beta 2$ -nicotinic acetylcholine receptor partial agonist. *J. Med. Chem.* **2011**, *54*, 7588–7601. [[CrossRef](#)]

32. Bolchi, C.; Valoti, E.; Gotti, C.; Fasoli, F.; Ruggeri, P.; Fumagalli, L.; Binda, M.; Mucchietto, V.; Sciacaluga, M.; Budriesi, R.; et al. Chemistry and pharmacology of a series of unichiral analogues of 2-(2-pyrrolidinyl)-1,4-benzodioxane, prolinol phenyl ether, and prolinol 3-pyridyl ether designed as  $\alpha 4\beta 2$ -nicotinic acetylcholine receptor agonists. *J. Med. Chem.* **2015**, *58*, 6665–6677. [[CrossRef](#)]
33. Bavo, F.; Pallavicini, M.; Gotti, C.; Appiani, R.; Moretti, M.; Colombo, S.F.; Pucci, S.; Viani, P.; Budriesi, R.; Renzi, M.; et al. Modifications at C(5) of 2-(2-pyrrolidinyl)-substituted 1,4-benzodioxane elicit potent  $\alpha 4\beta 2$  nicotinic acetylcholine receptor partial agonism with high selectivity over the  $\alpha 3\beta 4$  subtype. *J. Med. Chem.* **2020**, *63*, 15668–15692. [[CrossRef](#)] [[PubMed](#)]
34. Eaton, J.B.; Peng, J.-H.; Schroeder, K.M.; George, A.A.; Fryer, J.D.; Krishnan, C.; Buhlman, L.; Kuo, Y.-P.; Steinlein, O.; Lukas, R.J. Characterization of human  $\alpha 4\beta 2$ -nicotinic acetylcholine receptors stably and heterologously expressed in native nicotinic receptor-Null SH-EP1 human epithelial cells. *Mol. Pharmacol.* **2003**, *64*, 1283–1294. [[CrossRef](#)]
35. Xiao, Y.; Kellar, K.J. The comparative pharmacology and up-regulation of rat neuronal nicotinic receptor subtype binding sites stably expressed in transfected mammalian cells. *J. Pharmacol. Exp. Ther.* **2004**, *310*, 98–107. [[CrossRef](#)] [[PubMed](#)]
36. Hansen, C.P.; Jensen, A.A.; Christensen, J.K.; Balle, T.; Liljefors, T.; Frølund, B. Novel acetylcholine and carbamoylcholine analogues: Development of a functionally selective  $\alpha 4\beta 2$  nicotinic acetylcholine receptor agonist. *J. Med. Chem.* **2008**, *51*, 7380–7395. [[CrossRef](#)]
37. Jensen, A.A.; Mikkelsen, I.; Frølund, B.; Bräuner-Osborne, H.; Falch, E.; Krogsgaard-Larsen, P. Carbamoylcholine homologs: Novel and potent agonists at neuronal nicotinic acetylcholine receptors. *Mol. Pharmacol.* **2003**, *64*, 865. [[CrossRef](#)]
38. Garvey, D.S.; Wasicak, J.T.; Decker, M.W.; Brioni, J.D.; Buckley, M.J.; Sullivan, J.P.; Carrera, G.M.; Holladay, M.W.; Arneric, S.P.; Williams, M. Novel isoxazoles which interact with brain cholinergic channel receptors have intrinsic cognitive enhancing and anxiolytic activities. *J. Med. Chem.* **1994**, *37*, 1055–1059. [[CrossRef](#)] [[PubMed](#)]
39. Wei, Z.-L.; Xiao, Y.; Yuan, H.; Baydyuk, M.; Petukhov, P.A.; Musachio, J.L.; Kellar, K.J.; Kozikowski, A.P. Novel pyridyl ring C5 substituted analogues of epibatidine and 3-(1-methyl-2(S)-pyrrolidinylmethoxy)pyridine (A-84543) as highly selective agents for neuronal nicotinic acetylcholine receptors containing  $\beta 2$  subunits. *J. Med. Chem.* **2005**, *48*, 1721–1724. [[CrossRef](#)]
40. Zwart, R.; Carbone, A.L.; Moroni, M.; Bermudez, I.; Mogg, A.J.; Folly, E.A.; Broad, L.M.; Williams, A.C.; Zhang, D.; Ding, C.; et al. Sazetidide-A is a potent and selective agonist at native and recombinant  $\alpha 4\beta 2$  nicotinic acetylcholine receptors. *Mol. Pharmacol.* **2008**, *73*, 1838–1843. [[CrossRef](#)]
41. Xiao, Y.; Fan, H.; Musachio, J.L.; Wei, Z.-L.; Chellappan, S.K.; Kozikowski, A.P.; Kellar, K.J. Sazetidide-A, a novel ligand that desensitizes  $\alpha 4\beta 2$  nicotinic acetylcholine receptors without activating them. *Mol. Pharmacol.* **2006**, *70*, 1454–1460. [[CrossRef](#)]
42. Young, G.T.; Broad, L.M.; Zwart, R.; Astles, P.C.; Bodkin, M.; Sher, E.; Millar, N.S. Species selectivity of a nicotinic acetylcholine receptor agonist is conferred by two adjacent extracellular  $\beta 4$  amino acids that are implicated in the coupling of binding to channel gating. *Mol. Pharmacol.* **2007**, *71*, 389–397. [[CrossRef](#)]
43. Tuan, E.W.; Horti, A.G.; Olson, T.T.; Gao, Y.; Stockmeier, C.A.; Al-Muhtasib, N.; Bowman Dalley, C.; Lewin, A.E.; Wolfe, B.B.; Sahibzada, N.; et al. AT-1001 is a partial agonist with high affinity and selectivity at human and rat  $\alpha 3\beta 4$  nicotinic cholinergic receptors. *Mol. Pharmacol.* **2015**, *88*, 640–649. [[CrossRef](#)] [[PubMed](#)]
44. Elliott, R.L.; Kopecka, H.; Gunn, D.E.; Lin, N.-H.; Garvey, D.S.; Ryther, K.B.; Holladay, M.W.; Anderson, D.J.; Campbell, J.E.; Sullivan, J.P.; et al. 2-(Aryloxymethyl) azacyclic analogues as novel nicotinic acetylcholine receptor (nAChR) ligands. *Bioorg. Med. Chem. Lett.* **1996**, *6*, 2283–2288. [[CrossRef](#)]
45. Schrödinger Release 2019-4: *Maestro*; Schrödinger LLC: New York, NY, USA, 2019.
46. Schrödinger Release 2019-4: *LigPrep*; Schrödinger LLC: New York, NY, USA, 2019.
47. Schrödinger Release 2019-4: *Protein Preparation Wizard*; *Epik*; Schrödinger LLC: New York, NY, USA, 2019; *Impact*; Schrödinger LLC: New York, NY, USA; *Prime*; Schrödinger LLC: New York, NY, USA, 2019.
48. Madhavi Sastry, G.; Adzhigirey, M.; Day, T.; Annabhimoju, R.; Sherman, W. Protein and ligand preparation: Parameters, protocols, and influence on virtual screening enrichments. *J. Comput. Aided Mol. Des.* **2013**, *27*, 221–234. [[CrossRef](#)] [[PubMed](#)]
49. Sherman, W.; Day, T.; Jacobson, M.P.; Friesner, R.A.; Farid, R. Novel procedure for modeling ligand/receptor induced fit effects. *J. Med. Chem.* **2006**, *49*, 534–553. [[CrossRef](#)]
50. Sievers, F.; Wilm, A.; Dineen, D.; Gibson, T.J.; Karplus, K.; Li, W.; Lopez, R.; McWilliam, H.; Remmert, M.; Söding, J.; et al. Fast, scalable generation of high-quality protein multiple sequence alignments using Clustal Omega. *Mol. Syst. Biol.* **2011**, *7*, 539. [[CrossRef](#)] [[PubMed](#)]
51. UniProt Consortium. UniProt: The universal protein knowledgebase in 2021. *Nucleic Acids Res.* **2021**, *49*, D480–D489. [[CrossRef](#)] [[PubMed](#)]
52. Larsson, A. AliView: A fast and lightweight alignment viewer and editor for large datasets. *Bioinformatics* **2014**, *30*, 3276–3278. [[CrossRef](#)] [[PubMed](#)]
53. Friesner, R.A.; Murphy, R.B.; Repasky, M.P.; Frye, L.L.; Greenwood, J.R.; Halgren, T.A.; Sanschagrin, P.C.; Mainz, D.T. Extra precision glide: Docking and scoring incorporating a model of hydrophobic enclosure for protein-ligand complexes. *J. Med. Chem.* **2006**, *49*, 6177–6196. [[CrossRef](#)] [[PubMed](#)]
54. Schrödinger Release 2019-4: *MacroModel*; Schrödinger LLC: New York, NY, USA, 2019.
55. Kores, K.; Lešnik, S.; Bren, U.; Janežič, D.; Konc, J. Discovery of novel potential human targets of resveratrol by inverse molecular docking. *J. Chem. Inf. Modeling* **2019**, *59*, 2467–2478. [[CrossRef](#)] [[PubMed](#)]